ELSEVIER

Physica D 157 (2001) 251–282

PHYSICA D

www.elsevier.com/locate/physd

Chaotic breather formation, coalescence, and evolution to energy equipartition in an oscillatory chain

V.V. Mirnov [a], A.J. Lichtenberg [a,*], H. Guclu [b]

[a] *Electrical Engineering and Computer Science Department, University of California, Berkeley, CA 94720-1770, USA*
[b] *Physics Department, Middle East Technical University, Ankara 06531, Turkey*

Received 2 October 2000; received in revised form 7 May 2001; accepted 7 June 2001
Communicated by E. Kostelich

Abstract

We study the formation and evolution of chaotic breathers (CBs) on the Fermi–Pasta–Ulam oscillator chain with quartic nonlinearity (FPU-β system). Starting with most of the energy in a single high-frequency mode, the mode is found to breakup on a fast time scale into a number of spatially localized structures (CBs) which, on a slower time scale, coalesce into a single CB. On a usually longer time scale, depending strongly on the energy, the CB gives up its energy to lower frequency modes, approaching energy equipartition among modes. We analyze the behavior, theoretically, using an envelope approximation to the discrete chain of oscillators. For fixed boundaries, periodic nonlinear solutions are found. The numerical structures formed after the fast breakup are found to approximate the underlying equilibrium. These structures are shown, theoretically, to undergo slow translational motions, and an estimated time for them to coalesce into a single chaotic breather are found to agree with the numerically determined scaling $\tau_B \propto E^{-1}$. A previously developed theory of the decay of the CB amplitude to approach equipartition is modified to explicitly consider the interaction of the breather with background modes. The scaling to equipartition of $T_{eq} \propto E^{-2}$ agrees with the numerical scaling and gives the correct order of magnitude of T_{eq}.

Keywords: Chaotic breather; FPU-β system; Energy equipartition

1. Introduction

Coupled oscillator chains form good test systems for investigating energy exchange among degrees of freedom [1]. In particular, the Fermi–Pasta–Ulam (FPU) system, consisting of a set of equal masses coupled to nearest neighbors by nonlinear springs, has been extensively studied [1–11,14,18,19,25,26]. Starting with energy initially in a low-frequency mode, Fermi et al. [2] observed, for low energies, that the oscillators did not relax to the equipartition state, but displayed recurrences which were later explained in terms of beating among the system modes [1,3]. A theoretical prediction of a threshold to fast equipartition by mode overlap [4] was subsequently qualitatively confirmed by studies of energy thresholds required to give approximate equipartition among modes [5–7]. A weaker mechanism that also led to equipartition on a slower time scale has also been studied [8–10]. With

* Corresponding author.
E-mail address: ajl@eecs.berkeley.edu (A.J. Lichtenberg).

0167-2789/01/$ – see front matter
PII: S0167-2789(01)00315-3

initial energy in a low-frequency mode, it was shown in [9] that the resonant interaction of a few low-frequency modes can lead to a local superperiod beat oscillation that is stochastic, transferring energy to high-frequency modes by diffusion. With increasing local energy, there is a transition from exponentially slow transfer to a time scale that is inversely proportional to a power of the energy density.

The FPU-β system with quartic nonlinearity can be approximated, for low-frequency mode initial conditions, by the MKdV equation, which admits a soliton solution, that can become unstable with increasing energy [11,25]. This instability roughly coincides with the creation of stochastic layers in the beat oscillations [9]. The close connection between the development of stochastic layers in beat oscillations and instabilities in nonlinear structures was also noted for the discretized sine-Gordon equation, consisting of pendula coupled by linear springs [12,13]. In [12], it was numerically found that the breakup of a nonlinear structure, starting from a high-frequency mode initial condition, occurred at higher energy and on a slower time scale than from energy initially in a low-frequency mode.

A partial understanding of this increased stability came from a series of analyses of breather-like structures on discrete systems that admitted exact breather solutions [14–19,26,27]. High-frequency mode initial conditions have symmetry of neighboring oscillators close to that of localized breathers. The resulting dynamics consists of three stages. First, there is an initial fast stage in which the mode breaks up into a number of breather-like structures. Second, on a slower time scale, these structures coalesce into one large unstable structure. These structures have been called chaotic breathers (CBs) [18]. Since a single large CB closely approximates a stable breather, the final decay stage, toward equipartition, can be very slow. This behavior has been observed in oscillator chains approximating the Klein–Gordon equation with various force-laws [15–17,27], e.g., the discretized sine-Gordon equation [17], and, more relevantly for this paper, the FPU-β model [14,18,19,26]. In [14,18,26], the energy was placed in the highest frequency mode with strict alternation of the amplitudes from one oscillator to the next. This configuration is stable up to a particular energy beyond which a parametric instability occurs, leading to the events described above [14,18,26]. However, the nonlinear evolution does not depend on special initial conditions, but will generically evolve from any high-frequency mode initial condition that has predominantly the alternating amplitude symmetry [19]. One does not know, in this generic situation, whether there exists any true energy threshold to achieve equipartition, although there appears to be some numerical evidence for such a threshold in the discretized sine-Gordon system [12]. However, as discussed extensively with respect to low-frequency mode initial conditions, the practical thresholds refer to observable time scales [9,10]. From a phase-space perspective it is intuitively reasonable that for a large number of oscillators and not too low an initial energy, the generic set of initial conditions will lie in a chaotic layer, but the chaotic motion can remain close to a regular orbit for very long times [1]. The scaling with energy density of the time to equipartition has been estimated, for high-frequency initial conditions, from the interaction of beat modes [19] using a procedure developed to calculate the equipartition time from low-frequency initial conditions [20]. The result gave the numerically observed scaling but strongly underestimated the time, which is at least partially related to the transient formation of the breather [19].

Considerable insight into the behavior of a nonlinear oscillator chain, starting from high-frequency mode initial conditions, can be obtained by introducing an envelope function for the displacements of the oscillators. The initial conditions for the envelope only contain long wavelength perturbations. For the envelope function, an expansion is then possible to obtain a nonlinear partial differential equation (PDE) which approximates the behavior of the discrete system [21,22,28]. Low-order expansions of this type produce PDEs that have integrable solutions in the form of envelope solutions, analogous to the solutions produced from low-frequency initial conditions [21,28]. Higher order terms destroy the integrability, but some discretized oscillator chains can have localized exact breather solutions [16,17,27]. Thus we might expect the results, obtained from higher order expansions, to approximate breather solutions that may, however, be weakly unstable.

The envelope function expansion procedure has been applied to the FPU-β system to explore the nonlinear long wavelength solution, its modulation instability, the localization into proto-breathers, and their coalescence into a

single chaotic breather [22]. These results were mainly limited to the small-amplitude nonlinear solution, which therefore limited the range of applicability. The initial breakup of the high-frequency mode was also calculated only for periodic boundary conditions, i.e. for the highest mode number for which the initial envelope function is uniform [22,23]. These limitations led to results that, while qualitatively significant, do not agree quantitatively with numerical results in the usually explored energy density ranges or with oscillator chains with fixed ends [18,19].

In the following sections, we first present the basic equations of the chain in oscillator and normal mode forms. We then use expansions to obtain the envelope equation. Then, in Section 3, we obtain solutions of the envelope equations valid for arbitrary amplitude. In Section 4, we observe the fast numerical evolution of the discrete equations for a range of energies and initial periodicities of the envelope. Section 5 considers coalescence of the chaotic breathers that are formed in the relaxation process. In Section 6, the mode picture of the energy transfer mechanism is modified to specifically take into account the beating between background low amplitude modes and the breather, to obtain an estimate of the breather decay time.

2. Basic equation and initial conditions

The Hamiltonian function of the FPU-β model of N oscillators can be written in the form

$$H = \sum_{i=0}^{N} \left[\frac{1}{2} p_i^2 + \frac{1}{2}(q_{i+1} - q_i)^2 + \frac{\beta}{4}(q_{i+1} - q_i)^4 \right], \tag{1}$$

$$\frac{\mathrm{d}^2 q_i}{\mathrm{d}t^2} = q_{i+1} + q_{i-1} - 2q_i + \beta[(q_{i+1} - q_i)^3 - (q_i - q_{i-1})^3], \quad i = 1, 2, \ldots, N. \tag{2}$$

The dimensionless factor β is in a standard form traditionally used in publications for the FPU-β model. We choose $\beta = 0.1$ to correspond to previous papers and thus facilitate comparison with the results of other studies. The choice of β rescales the dimensionless variables and the energy of the system.

The Hamiltonian function (1) consists of quadratic part H_h which describes the harmonic oscillations, and anharmonic quartic potential proportional to β. With fixed boundaries a canonical transformation of H_h gives N independent normal modes P_j, Q_j

$$Q_j = \left(\frac{2\Omega_j}{N+1} \right)^{1/2} \sum_{i=1}^{N} \sin(kij) q_i, \tag{3}$$

$$P_j = \left(\frac{2}{\Omega_j (N+1)} \right)^{1/2} \sum_{i=1}^{N} \sin(kij)\, p_i, \tag{4}$$

such that the linear part of the Hamiltonian becomes

$$H_\mathrm{h} = \sum_{j=1}^{N} \frac{\Omega_j}{2} (P_j^2 + Q_j^2), \tag{5}$$

where

$$\Omega_j = 2 \sin\left(\frac{1}{2} kj \right), \quad k = \frac{\pi}{N+1}, \quad j = 1, 2, \ldots, N. \tag{6}$$

The reverse transformation is

$$q_i = \left(\frac{2}{N+1}\right)^{1/2} \sum_{j=1}^{N} \sin(kij) \frac{Q_j}{\Omega_j^{1/2}}, \tag{7}$$

$$p_i = \left(\frac{2}{N+1}\right)^{1/2} \sum_{j=1}^{N} \sin(kij) \Omega_j^{1/2} P_j. \tag{8}$$

Index i is used for functions describing oscillators, while j is used to label the variables related to the normal modes. Transformations (7) and (8) automatically satisfy boundary conditions $p_0 = p_{N+1} = q_0 = q_{N+1} = 0$.

For numerical integration, initial conditions are usually chosen such that at $t = 0$ only one or a few normal modes are excited. Due to the anharmonic coupling some energy is transferred throughout the spectrum.

To excite specifically, a single normal mode with the frequency Ω_γ, the displacements of the oscillators and their momenta are chosen at $t = 0$ in accordance with (7) and (8). The total energy E is shared between kinetic and potential parts of (5) such that if a fraction f is delivered to the kinetic energy $P_\gamma^2(0) = 2fE/\Omega_\gamma$, the rest is placed in the potential energy

$$Q_\gamma^2(0) = \frac{1}{6\beta\Omega_\gamma} \left(\sqrt{24\beta E(1-f)(N+1) + (N+1)^2} - N - 1 \right). \tag{9}$$

Expression (9) is calculated with the help of (1) and takes into account the anharmonic term not included in (5). Correspondingly, the initial displacements and velocities of the oscillators are as follows:

$$q_i(0) = \left(\frac{2Q_\gamma^2(0)}{\Omega_\gamma(N+1)}\right)^{1/2} (-1)^{i+1} \sin\left(\frac{\pi i n}{N+1}\right), \tag{10}$$

$$\dot{q}(0) = p_i(0) = \left(\frac{2P_\gamma^2(0)\Omega_\gamma}{N+1}\right)^{1/2} (-1)^{i+1} \sin\left(\frac{\pi i n}{N+1}\right). \tag{11}$$

We will mostly treat the case $N = 128$ with initially excited mode $\gamma = 120$. We principally examine cases with γ in the upper part of the spectrum so that $n = N + 1 - \gamma \ll N + 1$. Note that for these cases, the characteristic times of the initially excited modes correspond to a period $T \simeq \pi$, e.g., the frequency $\Omega_{120} \simeq 2$. In numerical calculations, a small fraction of the total energy (10%) is usually placed into two satellites $\gamma - 1$ and $\gamma + 1$ to speed up the initial phase of the relaxation; however, this does not play an important role in long term behavior of the system.

A typical profile of initial displacements (10) is shown in Fig. 1 for the case $E = 50$, $f = 0$, $\gamma = 120$, exhibiting the fast variations of q_i from one oscillator to another characteristic of high γ modes. As in previous studies [21,22,28], to remove this fast variations we introduce the envelope function $\psi_i(t) = (-1)^i q_i(t)$ which is a slowly varying function of the number i. The profile of the complete envelope function corresponding to Fig. 1 is illustrated in Fig. 2. The smooth spatial profile of ψ makes possible the use of a continuous approximation where the oscillators are described by the continuous variable $x = ai$, where a is the lattice period. Taylor's expansion then gives

$$\psi(x \pm a) = \psi(x) + \psi_x(x)(\pm a) + \tfrac{1}{2}\psi_{xx}(x)a^2 + \tfrac{1}{16}\psi_{xxx}(x)(\pm a)^3 + \tfrac{1}{24}\psi_{xxxx}(x)a^4 + \cdots. \tag{12}$$

Substituting (12) in (2) and collecting terms proportional to the different powers of a yields

$$\begin{aligned} \psi_{tt} &+4\psi + 16\beta\psi^3 + a^2\{\psi_{xx} + \beta(12\psi\psi_x^2 + 12\psi^2\psi_{xx})\} + a^4\{\tfrac{1}{12}\psi_{xxxx} + \beta(3\psi_x^2\psi_{xx} \\ &+3\psi\psi_{xx}^2 + 4\psi\psi_x\psi_{xxx} + \psi^2\psi_{xxxx})\} + \cdots = 0, \end{aligned} \tag{13}$$

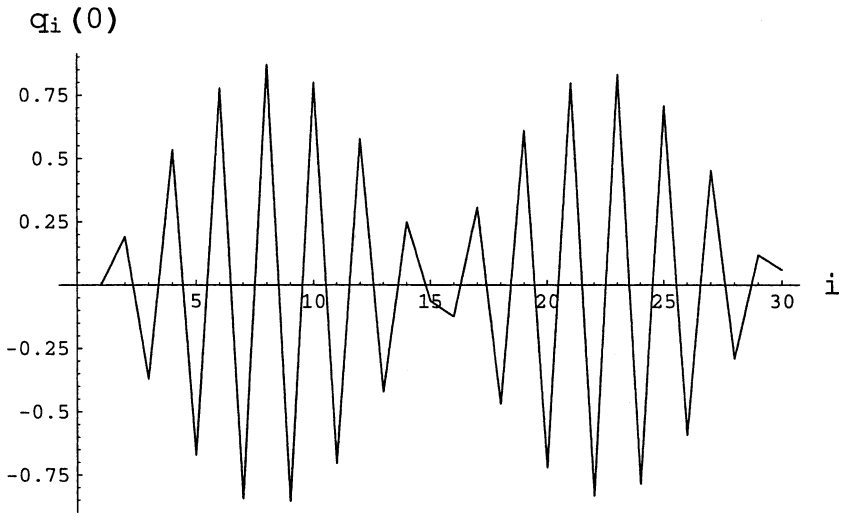

Fig. 1. Initial displacements q_i for the first 30 oscillators ($i = 1, 2, \ldots, 30$) out of $N = 128$ in the case $E = 50$, $\gamma = 120$, $n = N + 1 - \gamma = 9$. The mode has the symmetry that left and right oscillators (with respect to the central one) have displacements of almost equal amplitude but opposite sign.

where subscripts t and x stand for temporal and spatial derivatives of $\psi(x, t)$. Linear terms with spatial derivatives describe the dispersion (dependence of Ω on effective wavenumber $\pi j/(N + 1)$ in (6)), while the nonlinear terms produce a frequency shift, which drives a process of steepening of the envelope function. The combination results in formation of localized states (CBs). This qualitatively explains why relaxation is accompanied by the formation of sharply localized states if energy is initially deposited in the high-frequency part of the spectrum where the effect of

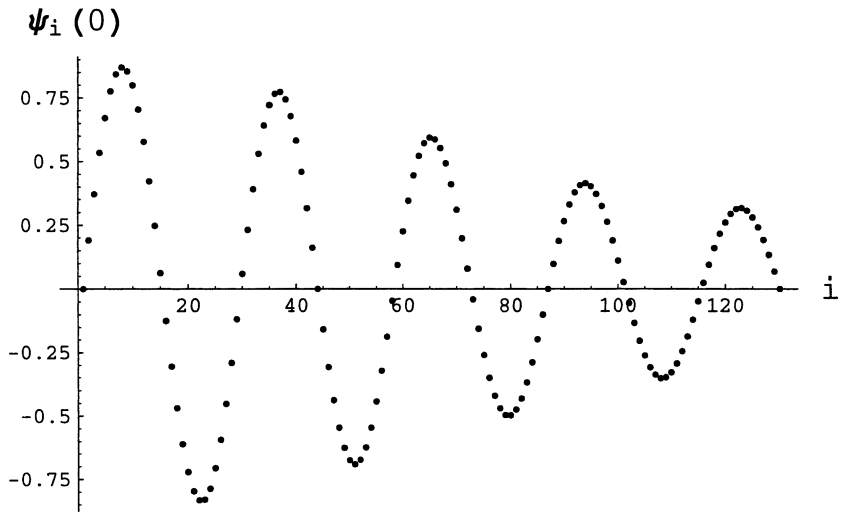

Fig. 2. The plot of the envelope function $\psi_i = (-1)^i q_i(0)$ at initial time $t = 0$, $N = 128$, $\gamma = 120$. Nine extrema correspond to $n = N+1-\gamma = 9$. The smooth decrease of ψ_i from left to right results from the fact that in numerical simulations a small amount of energy ($\sim 10\%$) was placed in two nearest neighbor modes $\gamma = 119$ and 121.

dispersion is small, while only broad nonlinear structures are formed if the energy is initially in the low-frequency modes where the dispersion is large.

3. Solutions for the envelope function

In (13), keeping terms up to the fourth power of a, introducing the dimensionless variable $x \to x/a$ ($0 \le x \le N+1$) and assuming a monochromatic dependence $\psi(x,t) = \psi(x)\cos\omega t$ leads to an approximate equation for $\psi(x)$

$$(-\omega^2+4)\psi + \psi_{xx} + \beta(12\psi^3 + 9\psi\psi_x^2 + 9\psi^2\psi_{xx}) + \tfrac{1}{12}(\psi_{xxxx} + \beta(27\psi_x^2\psi_{xx} + 27\psi\psi_{xx}^2 + 36\psi\psi_x\psi_{xxx} + 9\psi^2\psi_{xxxx})) = 0, \tag{14}$$

where we have used the rotating wave approximation (RWA) $\cos^3\omega t = \frac{3}{4}\cos\omega t + \frac{1}{4}\cos 3\omega t$, dropping terms proportional to $\cos 3\omega t$ [21,22,28]. Neglecting terms proportional to β yields a linear equation for the eigenmodes:

$$(-\omega^2+4)\psi + \psi_{xx} = 0. \tag{15}$$

Solving this equation for $\psi(x)$ with zero boundary conditions at $x = 0$ and $x = N+1$ gives a set of eigenmodes which correspond to the high-frequency linear normal modes of the discrete FPU chain

$$\psi_n^{(0)}(x) = \psi_{m_n}\sin q_n x, \tag{16}$$

$$\omega^2 = 4 - q_n^2, \quad q_n = \frac{\pi(N+1-\gamma)}{N+1} = \frac{\pi n}{N+1} \tag{17}$$

with $\psi_{m_n} \equiv \psi_{\max,n}$, where $n = N+1-\gamma \ll N+1$. Superscript (0) indicates that (16) is a solution to the linearized equation (15).

The reduced (with all terms of order a^4 dropped) nonlinear equation (14) has exact analytical solutions, $\psi(x)$, which are periodic functions of x. A subset of these solutions have $q = 0$ at $x = 0, N+1$, which are a natural generalization of the linear solutions for the case when nonlinear effects are important. These envelope functions have the same spatial periodicity as the corresponding linear modes (16). However, their profiles are not sinusoidal and the frequency of oscillations has a nonlinear shift. Multiplying (14) by ψ_x, and integrating over x yields a first integral

$$(-\omega^2+4)\psi^2 + \psi_x^2 + \beta(6\psi^4 + 9\psi^2\psi_x^2) = C_1, \tag{18}$$

where all terms of order a^4 have been dropped.

This function describes a family of solutions which depends on two parameters, C_1 and ω. Eq. (18) has been examined in the special case, where C_1 is chosen such that $\psi_x = 0$ at $\psi = \psi_{\max}$ and $\psi = \psi_{\min}$ [22]. We consider more general cases assuming that $\psi_x = 0$ at $\psi = \psi_{\max}$ but not necessarily at $\psi = \psi_{\min}$ (see, e.g., solution (16) for $n = 1$). Normalizing $\psi(x)$ to the maximum value $\psi_m \equiv \psi_{\max}$, and introducing a new function $f(x) \equiv \psi(x)/\psi_m$ one can rewrite (18) in the form of energy conservation for a particle in a potential $U(f)$

$$\tfrac{1}{2}f_x^2 + U(f) = 0, \tag{19}$$

where f_x^2 plays role of kinetic energy,

$$U(f) = -\frac{3\beta\psi_m^2(1-f^2)(f^2+C_2)}{(1+9\beta\psi_m^2 f^2)}, \tag{20}$$

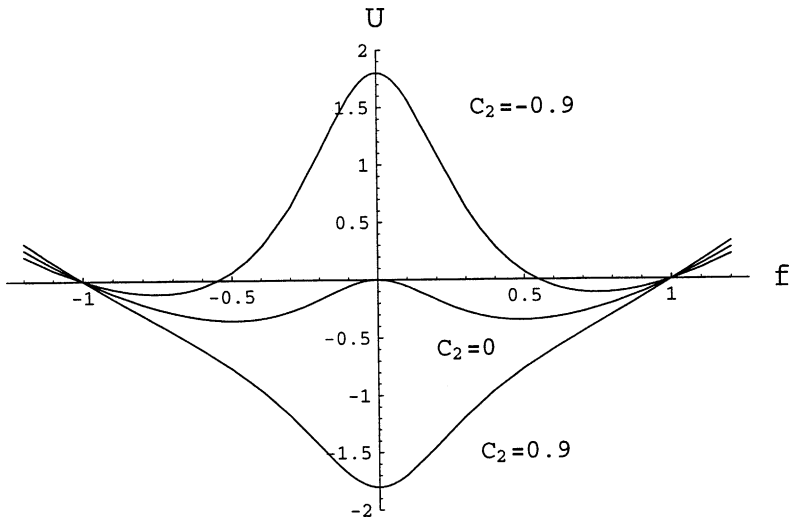

Fig. 3. Graphs of the effective potential energy $U(f)$ as a function of f, $0 \le f \le 1$, for three values of the constant of integration C_2.

and the total energy is zero. In transforming from (18) to (19), (20) the relation $f_x = 0$ at $f = 1$ is used and a new constant $C_2 = (4 - \omega^2 + 6\beta\psi_m^2)/6\beta\psi_m^2$ is introduced, with $C_1 = 6\beta\psi_m^4 C_2$. The graphs of $U(f)$ are illustrated in Fig. 3, for three different values of the constant C_2 ($C_2 = -0.9, 0, 0.9$). Intersections of these graphs with the horizontal line $E = 0$ show that in the case of positive C_2 (e.g., $C_2 = 0.9$) solutions $\psi(x)$ are oscillating functions of x which vary between minimum $-\psi_m$ and maximum ψ_m values. $C_2 = 0$ corresponds to the special separatrix solution which is represented by the single localized breather with $\psi(x) \to 0$ at $x \to \pm\infty$ and frequency

$$\omega_B^2 = 4 + 6\beta\psi_m^2. \tag{21}$$

For negative C_2 solutions $\psi(x)$ vary between two nonzero positive/negative boundaries $\psi_{\max}$ and $\psi_{\min}$ with frequency $\omega^2 = 4+6\beta(\psi_{\min}^2+\psi_{\max}^2)$. This third family of solutions is related to the case of periodic nonzero boundary conditions, $q_1 = q_{N+1}$, mentioned above. In particular, $C_2 = -1$, is the π mode for which each oscillator has opposite phase and equal amplitude as its neighbors; correspondingly, the envelope function $\psi = \psi_{\max} = \psi_{\min} = \psi_m$. In this case, the nonlinear frequency shift reaches a maximum value

$$\omega^2 = 4 + 12\beta\psi_m^2. \tag{22}$$

To satisfy boundary conditions of zero displacements at $x = 0$ and $x = N+1$, the first case (positive C_2) is required since it is the one which periodically passes though the point where $\psi = 0$. The spatial period of these oscillations is given by

$$\int_0^1 \mathrm{d}f \left(\frac{\mathrm{d}f}{\mathrm{d}x}\right)^{-1} = \frac{\Lambda}{4}. \tag{23}$$

The dispersion relation (23) determines the spectrum of the frequencies ω as a function of n and ψ_m. Substituting f_x from (19) in (23) and using a new variable $\sin\alpha = f$, (23) can be written in the form

$$I(r, \psi_m) = \frac{2}{\pi}\int_0^{\pi/2} \mathrm{d}\alpha \left(\frac{1 + 9\beta\psi_m^2 \sin^2\alpha}{\sin^2\alpha + r^2}\right)^{1/2} = \sqrt{6\beta\psi_m^2\left(\frac{N+1}{\pi n}\right)^2}, \tag{24}$$

where we have substituted $\frac{1}{4}\lambda = (N+1)/2n$ on the RHS. The factor $r^2 \equiv C_2 = (4-\omega^2+6\beta\psi_m^2)/6\beta\psi_m^2$ has been introduced as a positive quantity to insure convergence of the integral. The parameter

$$w(n,\psi_m) = 6\beta\psi_m^2\left(\frac{N+1}{\pi n}\right)^2 \tag{25}$$

on the RHS of (24) gives the relative effect of the nonlinear frequency shift to the linear frequency shift.

In the case of weak nonlinearity with $w \ll 1$, w is balanced by the integral in the LHS with $r \gg 1$. In this limit, $I(r,\psi_m) \propto 1/r$, yielding a discrete spectrum of eigenfrequencies

$$\omega_n^2 = 4 + 6\beta\psi_m^2 - \frac{\pi^2 n^2}{(N+1)^2} \tag{26}$$

with the nonlinear correction $6\beta\psi_m^2$ added to the linear case (17). In the opposite limiting case, $w(n,\psi_m) \gg 1$, w is balanced by the LHS if $r \ll 1$. Asymptotically, expanding the LHS for $r \ll 1$ yields a logarithmic dependence on r in the leading approximation of $I(r,\psi_m)$ (A.2). Substituting (A.3) in (24) yields the spectrum of the eigenfrequencies valid in the case of strong nonlinearity

$$\omega_n^2 = 4 + 6\beta\psi_m^2\left\{1 - \frac{16}{1+9\beta\psi_m^2}\exp\left[-\sqrt{6\beta\psi_m^2}\left(\frac{N+1}{n} - \sqrt{6}\arcsin\sqrt{\frac{9\beta\psi_m^2}{1+9\beta\psi_m^2}}\right)\right]\right\}. \tag{27}$$

The factor r^2 is given by the second term in curly brackets, which is exponentially small, $r^2 \propto \exp(-w/\pi)$.

The spatial profiles of the nonlinear eigenfunctions $\psi(x)$ are determined by integrating (19) and (20), having an upper limit given by $\arcsin(\psi/\psi_m)$ and zero boundary condition at $x = 0$,

$$x(\psi) = \frac{1}{\sqrt{6\beta\psi_m^2}}\int_0^{\arcsin(\psi/\psi_m)} \mathrm{d}\alpha\left(\frac{1+9\beta\psi_m^2\sin^2\alpha}{\sin^2\alpha + r^2}\right)^{1/2}, \quad 0 \le x \le \tfrac{1}{4}\Lambda. \tag{28}$$

Eq. (28) defines $\psi(x)$ in $0 \le x \le \frac{1}{4}\Lambda$. It is symmetrically continued from $\frac{1}{4}\Lambda$ to $\frac{1}{2}\Lambda$, then antisymmetrically reflected from $\frac{1}{2}\Lambda$ to Λ, and periodically continued over the entire chain. The resulting graphs of $\psi_n(x)$ are plotted in Fig. 4a and b together with the profiles of equivalent linear modes (16) for typical values $N = 128$, $n = 9$, $\beta = 0.1$ and two amplitudes $\psi_m = 0.45$ and $\psi_m = 1.85$, respectively. These values correspond to relatively weak and relatively strong nonlinearity, $w(9,\psi_m) \simeq 3$ and $w(9,\psi_m) \simeq 50$, respectively (note that (26) is not satisfied for $w \simeq 3$, so the solution from (24) is used). The linear profiles (16) are used as initial conditions in numerical studies. In the process of relaxation, these initial profiles might be expected to approach the equivalent envelope solutions (28) of the same periodicity and total energy. Due to conservation of energy, the amplitudes of the envelope solutions (28) are higher than the initial values. In the weakly nonlinear case (a) the difference is small, while in the strongly nonlinear case (b) the difference is large because the nonlinear peaks are much narrower than the initial sinusoidal profiles. Numerical calculations presented in the next section show that the periodicity may be broken in the process of relaxation such that the only link between initial and final states is the conservation of energy. The periodic envelope solution (28) with $n = 1$ looks similar to the single breather in an infinitely long chain, which is obtained from (28) in the limit $N \to \infty$. Putting $r = 0$ and rearranging the limits of integration in accordance with zero boundary conditions at infinity, yields

$$x(f) = \frac{1}{\sqrt{6\beta\psi_m^2}}\int_{\arcsin f}^{\pi/2}\frac{\mathrm{d}\alpha}{\sin\alpha}(1+9\beta\psi_m^2\sin^2\alpha)^{1/2}, \quad 0 \le x < +\infty. \tag{29}$$

For the low amplitude case, $9\beta\psi_m^2 \ll 1$, integral (29) is simplified giving

$$\psi_{\mathrm{B}}(x) = \psi_m\cosh^{-1}(\sqrt{6\beta}\psi_m x), \tag{30}$$

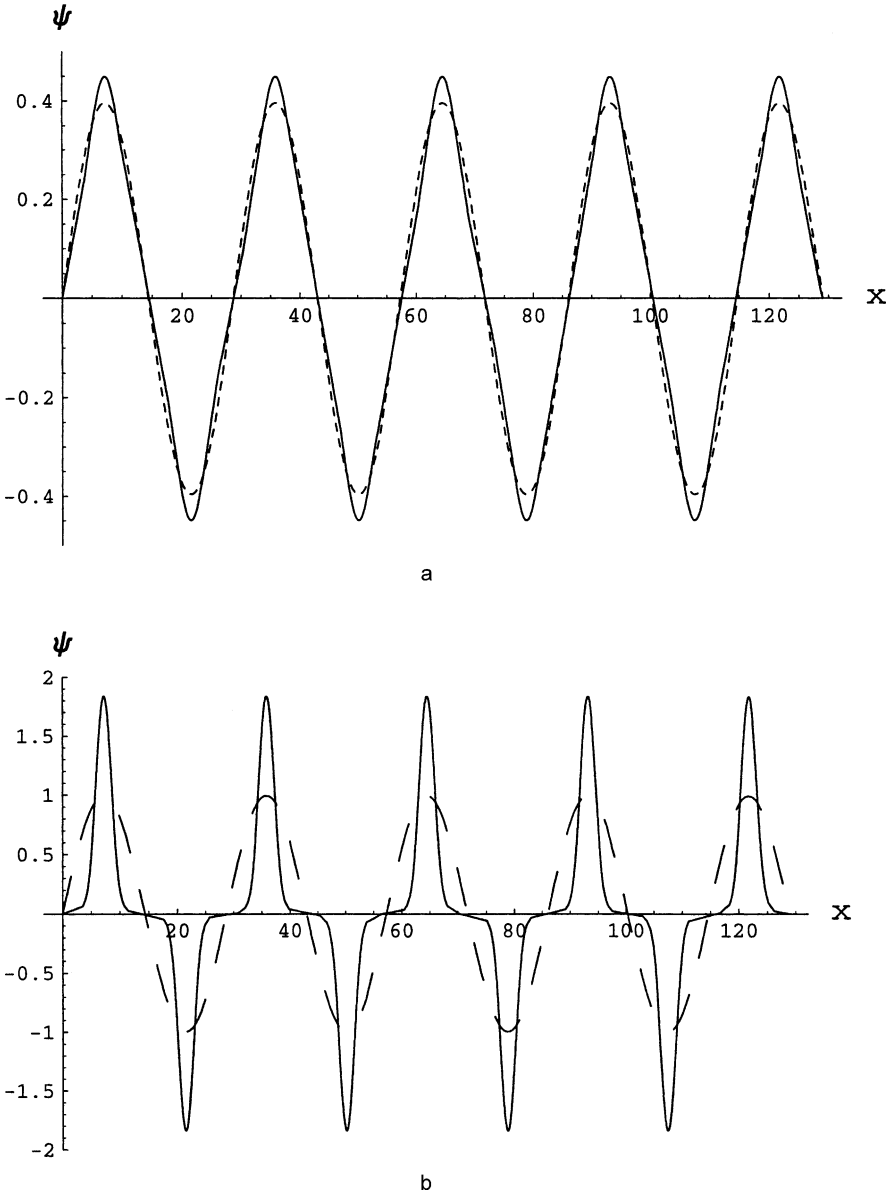

Fig. 4. (a) Comparison of the weakly nonlinear envelope solution (28) (solid line) with the equivalent profile of the normal mode (16) (dashed line) with energy $E = 20$ and symmetry $n = 9$. Since the factor $w \simeq 3$ is not too large, the curves are close to each other. (b) Comparison of the strongly nonlinear envelope solution (28) (solid line) with the equivalent profile of the normal mode (16) (dashed line) at energy $E = 200$ and symmetry $n = 9$. The large value of $w \simeq 50$ makes the curves significantly different.

while in the large amplitude case, $9\beta\psi_m^2 \gg 1$, (29) describes, asymptotically, the breather of finite width $d \simeq 5$ (five oscillators)

$$\psi_{\mathrm{B}}(x) = \psi_m \cos\sqrt{\tfrac{2}{3}}x, \qquad -\pi\sqrt{\tfrac{3}{8}} < x < \pi\sqrt{\tfrac{3}{8}}. \tag{31}$$

The energy of the envelope solutions is given by Eq. (B.4). The first two terms are calculated at the boundaries and cancel each other because of the spatial periodicity of the modes. Substituting (18) and (19) into (B.4), expressing ω^2 in terms of r^2 and transforming the variable of integration as in (24) yields an expression for the energy

$$E = \frac{2n\psi_m}{\sqrt{6\beta}} \int_0^{\pi/2} \mathrm{d}\alpha \left(\frac{1 + 9\beta\psi_m^2 \sin^2\alpha}{\sin^2\alpha + r^2} \right)^{1/2} \left(3\beta\psi_m^2 \sin^4\alpha + 2\sin^2\alpha - \frac{3}{2}\beta\psi_m^2 r^2 \right). \tag{32}$$

The integral in (32) is simplified and calculated analytically in two limiting cases. If ψ_m is sufficiently high that, $w(n, \psi_m) \gg 1$, nonlinear effects are dominant in comparison with the effect of dispersion and according to (24), $r \to 0$. Substituting $r = 0$ in (32), the integral is calculated exactly and defines a function $Z(y)$ with $y = \beta\psi_m^2$. The explicit expression for $Z(y)$ is given by (B.5) and (B.6). Although we are only considering large nonlinear frequency shift (with respect to the dispersion), we still have subcases $y \gg 1$ and $y \ll 1$ which we call, respectively, large and small amplitude nonlinear envelopes. In the first, large amplitude subcase, the asymptotic expansion of $Z(y)$ yields

$$E = \frac{9\pi\sqrt{6}n\beta}{16} \left(\psi_m^4 - \frac{2}{3\pi\sqrt{\beta}} \psi_m^3 \right), \quad 1 \ll \sqrt{6\beta\psi_m^2}, \tag{33}$$

where the ψ_m^3 term is the next order correction to the leading ψ_m^4 term. The energy is mostly due to the quartic β term in the potential energy (1). The envelope function and energy are concentrated in n narrow periodically distributed peaks each consisting of 4–5 oscillators, while in wide areas between the peaks oscillations are exponentially small. In the second, small amplitude, subcase the leading terms in the expansion of $Z(y)$ yield

$$E = \frac{4n}{\sqrt{6\beta}} (\psi_m + 4\beta\psi_m^3), \quad \frac{\pi n}{N+1} \ll \sqrt{6\beta\psi_m^2} \ll 1, \tag{34}$$

where the ψ_m^3 term is the next order correction to the leading ψ_m term. The energy is mostly due to the quadratic term in the potential energy (1). It is also localized in n periodically distributed peaks but the width of the peaks and, correspondingly, the number of oscillators in each of them are inversely proportional to ψ_m. This results in the linear dependence on ψ_m in (34).

If the amplitude ψ_m is sufficiently low that $\sqrt{6\beta\psi_m^2} \ll \pi n/(N+1)$, the oscillations become nearly linear. As in obtaining (26), the factor r is now much greater than one and integral (32) can be calculated in the limit $r \to \infty$ yielding

$$\frac{E}{N+1} = \psi_m^2 \left(1 - \frac{\pi^2 n^2}{4(N+1)^2} \right), \quad \sqrt{6\beta\psi_m^2} \ll \pi n/(N+1) \ll 1. \tag{35}$$

The quadratic energy dependence on ψ_m again results from the quadratic term in the potential energy (1) with a maximum value of $2\psi_m^2$ in a single oscillator, and a factor of $\frac{1}{2}$ is introduced from the nonuniform profile of the envelope function. This regime is equivalent to the discreet normal mode solution, which represents initial conditions used in numerical calculations in the case when all energy is placed at $t = 0$ in the potential energy.

4. Fast evolution from initial states

For most numerical studies of oscillator chains, the initial state imposed on the system is mainly that of a single linear mode. This state is generally not close to an equilibrium. The initial state rapidly relaxes, governed by the nonlinear equations. The evolution may be influenced by the underlying stability of nearby equilibria, but cannot be analyzed directly as perturbations around those equilibria. It is also possible to prepare the initial conditions to

be close to an equilibrium and consequently to directly analyze linear stability, but the results of such an analysis, while interesting, are only indirectly relevant to our nonlinear evolution. We study that situation in a separate paper. Preliminary studies indicate that the CBs that are formed in the nonlinear processes are probably marginally stable, which accounts for their long-lived existence.

One special case that can be solved for the unstable motion is that of periodic boundary conditions with the energy placed in the highest frequency mode (the π-mode) [23]. For this case, the unperturbed envelope function is uniform (does not depend on x) which simplifies the analysis. Then in the limit of small f_m, $y \ll 1$, the values of the fastest growing wavenumber k_m and the corresponding growth rate s_m were found in [22] to be

$$k_m = \sqrt{12\beta}\psi_m, \qquad s_m = 3\beta\psi_m^2. \tag{36}$$

In the opposite limit of large amplitudes, $y \gg 1$, the fastest growing mode wavenumber and maximum growth rate can also be calculated, and are found to be

$$k_m = 1.23, \qquad s_m = 0.93\sqrt{\beta}\psi_m. \tag{37}$$

In contrast to the case of the low amplitude results in (36), at large amplitude k_m is independent of the amplitude and s_m is a linear function of ψ_m. Comparing (36) and (37) we see that the transition from small to large amplitude takes place at $\beta\psi_m^2 \simeq \frac{1}{9}$ that corresponds, for $\beta = 0.1$, to $\psi_m \simeq 1$.

The modulation instability of the more general envelope solutions obtained in Section 3 requires a more complicated analysis. We will present analytic results in a separate paper; numerical methods are used below to qualitatively understand the fast initial relaxation.

The numerical treatment of stability is based on integration of the 128 equations of motion (2) for a 128 oscillator chain, with initial conditions $q_i(0) = q_i^{(\mathrm{B})} + \delta q_i$, $p_i(0) = 0$. Functions $q_i^{(\mathrm{B})}$ describe the unperturbed breather profile and are chosen either from the continuous model in the form of approximation (30) for $\psi_m < 1$ or as a breather solution of the discrete FPU model for $\psi_m > 1$. Low and high amplitude initial profiles are centered in the middle of the chain at $x = 64.5$. In all cases small ($\simeq 10\%$) perturbations with the wavelength of the fastest growing mode from (36) or (37) are added at $t = 0$ to speed up the instability. The time of integration is chosen to be 10 times longer than the inverse growth rate from (36) or (37). Results of these calculations show no significant time variations of the initial profiles over a wide range of amplitudes, $0.1 < \psi_m < 10$. These numerical results confirm stability of the nonlinear envelope solutions (28) with $n = 1$. In the low amplitude limit, $w(n, \psi_m) < 1$, the inequality is equivalent to the condition of stability of the π-mode such that the breather would also be stable. The envelope solutions (28) with higher numbers of n, $n = 2, 3, \ldots$, consist of n peaks whose profiles are similar to single breathers if $w(n, \psi_m) \gg 1$ and n is not too high ($n < 25$–30). Thus, one can expect stability of the peaks with respect to short wavelength perturbations of their shape. For long wavelength perturbations, a new effect appears when the number of peaks per wavelength is significantly larger than one. In this case perturbations effectively feel the averaged (over x) value of the coefficients that leads to (36) and (37). This results in a long wavelength modulation instability, as in (36) and (37) for the π-mode, but with averaged values of coefficients. The long wavelength perturbations do not change the shape of individual peaks but lead to the modulation of the peak amplitudes. This long wavelength instability is illustrated in Fig. 5a and b where the energies of oscillators e_i are plotted for $n = 16$ and two initial conditions, $E = 5(\psi_m = 0.2)$ and $E = 20(\psi_m = 0.4)$, at $t = 11,800$ and 3500 s, respectively. Growing perturbations of initially equal amplitudes with the wavelength $\lambda = 64$ and 32 are well described by the theory if averaging is taken into account by reducing their amplitudes to $\psi_m = 0.1$ and 0.2.

Since the initial conditions of much numerical work are taken to be normal modes of the linear problem they are different from nonlinear envelope solutions at the same energy. Normal modes are wider and, therefore, their amplitudes, ψ_i, are less than the amplitudes of corresponding nonlinear solutions, ψ_m. If the value of the difference $\Delta\psi = \psi_m - \psi_i$ is not too large, $\Delta\psi/\psi_m \leq 0.4$, a relaxation takes place in the form of regular oscillations of $\psi(x, t)$

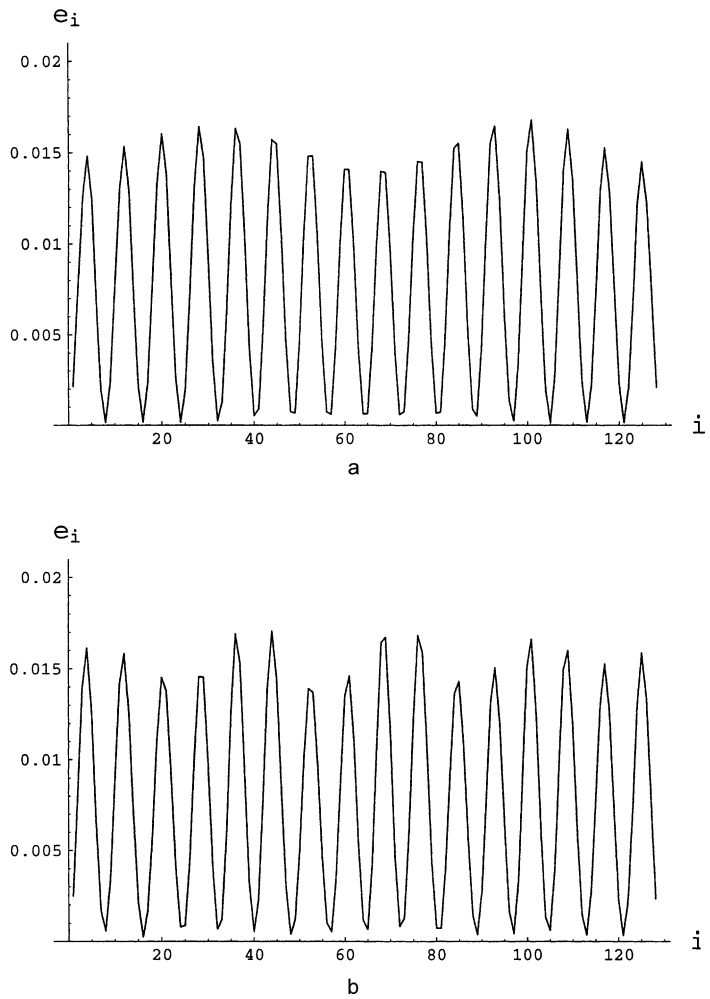

Fig. 5. Dynamics of the modulational instability of the periodic equilibrium with many peaks ($n \gg 1$). The curves show the profile of the normalized oscillator energies e_i versus i at a time when a long wavelength modulational instability is visible. (a) $E = 5, n = 16, t = 11,800$ s; the estimate of the most unstable wavelength, $\lambda_m = 64$, is in a good agreement with the observed wavelength. (b) $E = 20, n = 16, t = 3500$ s; the estimate of the most unstable wavelength, $\lambda_m = 32$, is in a good agreement with the observed wavelength.

around the equilibrium solution of the same symmetry of amplitude $\Delta\psi$. If $\Delta\psi$ is large, then the relaxation follows another scenario in which $\psi(x, t)$ oscillates around an envelope solution of a different symmetry with higher values of n. This process is more favorable because the equilibrium amplitude of an envelope solution with a higher value of n is lower and, therefore, closer to the initial amplitude at a given energy. A transition from a regular oscillation regime (with conservation of symmetry) to a breakup regime (with change of n) has a threshold depending on the initial amplitude or, equivalently, the energy of the initial state. The transition energy E_{tr} depends on the value of n of an initial normal mode. Numerical results show that the transition energy E_{tr}, starting from a normal mode, increases with n, approximately as n^2, provided n is not too large. This dependence can be explained qualitatively with the use of the nonlinear parameter w which gives a measure of the difference between strongly nonlinear and almost linear profiles of the envelope solutions. If $w \simeq 1$, the difference is of the order of 1 also, $\Delta\psi \simeq \psi_m$, which roughly corresponds to the transition from a regular to a breakup regime. From the above it follows that $\psi_{\mathrm{tr}} \propto n$ and $E_{\mathrm{tr}} \propto n^2$.

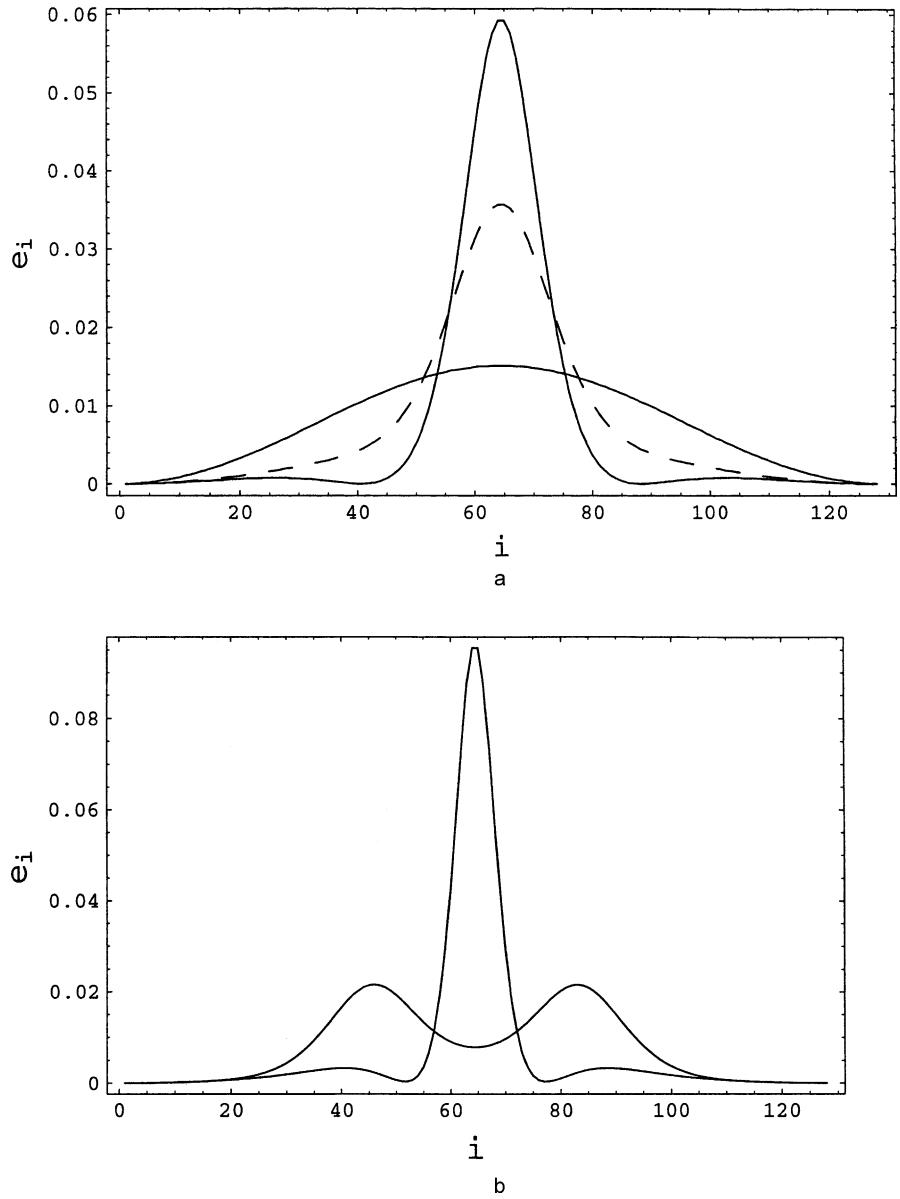

Fig. 6. Snapshots of oscillator energies e_i versus oscillator number i at successive times, illustrating the dynamics of relaxation from an initial state around the nearest equilibrium state. The dashed line shows the profile of the equilibrium envelope solution with the same initial energy and symmetry. (a) The case of regular oscillations without breakup of symmetry at low energy $E = 0.65$, $n = 1$; profiles of E_i are shown at $t = 0$ and 1800 s which correspond to the initial state and maximum of deviation of the envelope function from the initial state. (b) Illustration of the symmetry breaking at higher energy, $E = 1.29$, $n = 1$; the two distributions shown are the profile having initial symmetry at $t = 1000$ s and the transition to the symmetry $n = 2$ at $t = 2000$ s.

These conclusions are illustrated in Fig. 6 where snapshots of numerical results obtained at low energies and $n = 1$, initially, are given at two times. In Fig. 6a, the case of regular oscillations with $n = 1$ and $E = 0.65$ is shown. The energy of the individual oscillators are plotted versus i, with the equilibrium profile marked with a dashed line; the period of oscillations is $T = 4000$ s. This initial state is close to the transition to the breakup regime. The case

of a symmetry breaking oscillation for $n = 1$ but higher energy $E = 1.29$ is shown in Fig. 6b, where a periodic transition to the symmetry $n = 2$ is observed; the period of oscillation is $T \simeq 4500$ s.

For the usual initial condition of our numerical study, with the initial mode $\gamma = 120$, the initial modulation of the envelope is primarily as in Fig. 2. Depending on the energy this may or may not correspond to the "closest" underlying equilibrium. Since at high initial energies the relaxation process generally goes to a higher n-number, we therefore expect this initial condition to yield nine or more localized structures during the initial phase of rapid evolution. This is, in fact, what has been observed, with more structures developing at higher energies. These results bear further investigation over a wide range of initial conditions.

5. Breather coalescence

After a set of CBs have been formed, on a short time scale, by a modulational instability or breakup relaxation, the breathers coalesce, on a longer time scale, into a single chaotic breather. This process has been well documented, numerically [14,18,19,26], and the process has been studied in more detail in [22]. In fact, the physics is difficult to understand completely, and quantitative comparison with theory, as developed in [22], did not agree with detailed numerical results [19]. Our approach will be to follow the overall calculation program from [22], extended to include larger amplitude breathers where numerics can be conveniently carried out; then to examine, numerically, the various assumptions that enter into the calculations to see if theoretical estimates can be improved.

5.1. Analytical estimates

The basic physical notions are that some number of chaotic envelope breathers are formed, related to a combination of the fastest growing mode of the modulational instability, the initial condition symmetry, and relaxation process. These chaotic breathers are moving, in the manner of their low-frequency soliton cousins, and therefore collide with one another. Since the CBs are not exact nonlinear solutions to the underlying equations, they interchange energy in the interactions, and also take and lose energy against existing background modes. In a restricted situation, this process has been described theoretically [24], showing that energy is on average transferred from smaller to larger structures. The end result is then a single large structure. To estimate the time scale for the coalescence, the time scale τ_B is constructed as [22]

$$\tau_B \simeq \frac{l}{v_B} \simeq \frac{1}{n_B \sigma v_B}, \tag{38}$$

where v_B is the breather velocity, and the mean free path l is related in the usual way to the density of breathers n_B and the effective cross-section for absorption of colliding breathers σ. The calculation in [22] proceeds from Eq. (13) (without a^4 terms) in the form of Hamiltonian equations for $\Psi(x,t)$ and $\Psi^*(x,t)$ introduced through a complex amplitude function

$$\psi(x,t) = \tfrac{1}{2}(\Psi(x,t)\,\mathrm{e}^{-\mathrm{i}\omega t} + \Psi^*(x,t)\,\mathrm{e}^{\mathrm{i}\omega t}). \tag{39}$$

Dropping the terms with the second time derivatives ($\ddot{\Psi} \ll \omega\dot{\Psi}$) and using the RWA yields canonical Hamiltonian equations

$$\mathrm{i}\omega\dot{\Psi} = \frac{\delta\mathcal{H}}{\delta\Psi^*}, \qquad -\mathrm{i}\omega\dot{\Psi}^* = \frac{\delta\mathcal{H}}{\delta\Psi}, \tag{40}$$

where $\mathcal{H}$ is defined by $\mathcal{H} = \int H\,\mathrm{d}x$ with a Hamiltonian density

$$H = -\tfrac{1}{2}\{|\Psi_x|^2 - 6\beta|\Psi|^4 + 6\beta[|\Psi|^2|\Psi_x|^2 + \tfrac{1}{4}(\Psi^2\Psi^{*2} + \Psi^2\Psi^{*2})]\}. \tag{41}$$

Equations (40) describe slow variation of the envelope and they have the integrals of motion [24]

$$\mathcal{H} = \int H \, \mathrm{d}x, \qquad \mathcal{P} = -\frac{\mathrm{i}}{2} \int (\Psi \Psi_x^* - \Psi^* \Psi_x) \, \mathrm{d}x, \qquad \mathcal{N} = \int |\Psi|^2 \, \mathrm{d}x \tag{42}$$

the energy, momentum and number of quasi-particles, respectively. These results are then used to estimate v_B in (38) from the defining quantities in (42), which is evaluated in [22] within the approximation of a small amplitude traveling solution, with $N \to \infty$, to obtain

$$\Psi(x,t) = \psi_m \frac{\exp(\mathrm{i}kx - \mathrm{i}\Omega t)}{\cosh\left[\sqrt{6\beta}\psi_m (x - v_\mathrm{B} t)\right]}. \tag{43}$$

Expression (43) is not an exact solution to (40) but satisfies these equations for a reduced Hamiltonian (41) in which the last three terms are dropped. In this approximation, Ω is the solution to the dispersion relation $\Omega = (\frac{3}{2}\beta)\psi_m^2 - \frac{1}{4}k^2$ while the wave vector

$$k = -v_\mathrm{B}(\omega + \Omega) \simeq -2v_\mathrm{B}. \tag{44}$$

The velocity v_B plays role of the group velocity of the wave packet. Eq. (44) is equivalent to the usual relationship $v_\mathrm{B} = \partial\Omega/\partial k$ and defines k as a function of v_B. The value of v_B by itself is not defined in this approach and is considered as a free parameter. To define the values of v_B an additional argument is used in [22], that due to the interaction of quasi-particles trapped inside the breather quasi-equilibrium values of k and v_B are established, for which the Hamiltonian, $\mathcal{H} = 0$. In analogy with the classical oscillator this statement was called a "virial theorem". Applying this theorem v_B is found from (42) to be a linear function of the amplitude

$$v_\mathrm{B} = \sqrt{\frac{\beta}{2}}\psi_m. \tag{45}$$

Note that k in (44), using (45), is $k = \sqrt{2\beta}\psi_m$ which is not equal to $k_m = \sqrt{12\beta}\psi_m$ obtained in (36) for the fastest growing mode of the modulational instability, but has the same scaling. Continuing the argument from [22] the density of breathers n_B, as obtained from the modulational instability at small amplitude, is

$$n_\mathrm{B} \simeq \frac{k_\mathrm{max}}{2\pi} \simeq \frac{(3\beta)^{1/2}\psi_m}{3}, \tag{46}$$

and σ is taken from a Born approximation for weak scattering to have proportionality

$$\sigma \propto \left(\int U_\mathrm{int} \, \mathrm{d}x\right)^2 \propto \left(\int \psi_1 \psi_2 \, \mathrm{d}x\right)^2 \propto (\psi_m^2 d)^2 \propto \psi_m^2. \tag{47}$$

Substituting these scalings in (38) leads to the scaling $\tau_\mathrm{B} \propto \epsilon_\mathrm{B}^{-2}$, where $\epsilon_\mathrm{B} = E_\mathrm{B}/N$ is the energy density of the breathers. Recent numerical investigations of the time scale for coalescence, in an energy range that is easily accessible numerically, produced the scaling for the time required to obtain a single CB [19], $\tau_\mathrm{B} \propto \epsilon^{-1}$, in contradiction to the small amplitude result (more precisely $\tau_\mathrm{B} \propto E^{-1}$ since N was held constant).

Since numerical treatments mentioned above were mostly done for relatively large energies, the low amplitude scalings (45) and (47) are not applicable to this case and have to be extended to high amplitudes. We first reconsider the concept of breather velocity for high amplitude. For analysis of nonstationary envelopes, which describe relaxation, instability, or breather translational motion, we rewrite the basic equation (13) in the form of two-coupled equations for amplitude $q(x,t)$ and phase $\phi(x,t)$ which are related to $\psi(x,t)$ as

$$\psi(x,t) = q(x,t)\cos(\omega t + \phi(x,t)). \tag{48}$$

Substituting (48) in (13) and collecting terms proportional to $\sin(\omega t + \phi(x,t))$ and $\cos(\omega t + \phi(x,t))$ leads to coupled equations for the phase $\phi(x,t)$ and amplitude $q(x,t)$

$$q\phi_{tt} + 2q_t(\omega + \phi_t) + 2q_x\phi_x + q\phi_{xx} + 12\beta q^2 q_x\phi_x + 3\beta q^3\phi_{xx} = 0, \tag{49}$$

$$q_{tt} - (\omega + \phi_t)^2 q + 4q + q_{xx} - q\phi_x^2 + 12\beta q^3 + 9\beta q(qq_x)_x - 6\beta q^3\phi_x^2 = 0. \tag{50}$$

To analyze a moving breather, we will use (49) and (50) and choose solutions in the form $q(x,t) = q(x - ut)$, $\phi(x,t) = \phi(x - ut)$. Derivatives of these functions with respect to their arguments $\xi = x - ut$, are introduced as q' and ϕ'. Substituting these forms into (49) and (50) with $q_t = -uq'$, $\phi_t = -u\phi'$, yields two-coupled ordinary differential equations for ϕ and q

$$q(1 + u^2 + 3\beta q^2)\phi'' + 2q'(1 + u^2 + 6\beta q^2)\phi' = 2u\omega q', \tag{51}$$

$$(1 + u^2)q'' + (4 - \omega^2)q + 12\beta q^3 + 9\beta q(qq')' + 2\omega u\phi' q - (\phi')^2(1 + u^2 + 6\beta q^2)q = 0. \tag{52}$$

Eq. (51) is linear with respect to the first and second derivatives of ϕ and therefore has an exact solution (without singularity at $q = 0$)

$$\phi' = \frac{u\omega}{1 + u^2 + 3\beta q^2}. \tag{53}$$

Substituting (53) in (52), multiplying by q' and integrating over ξ yields a first integral

$$(1 + u^2 + 9\beta q^2)q'^2 + \left(4 - \omega^2 + \frac{\omega^2 u^2}{1 + u^2 + 3\beta q^2}\right) q^2 + 6\beta q^4 = 0, \tag{54}$$

where the constant of integration is chosen to be zero to provide zero boundary conditions at infinity. The frequency of the moving breather depends on its amplitude and velocity and can be obtained from (54) applied to the point $\xi = 0$, where the amplitude $q(\xi)$ reaches its maximum, q_m

$$\omega^2 = (4 + 6\beta q_m^2)\left(1 + \frac{u^2}{1 + 3\beta q_m^2}\right). \tag{55}$$

Making use of this result, (54) can be rewritten in the form of an energy conserving Hamiltonian $h = \frac{1}{2}q'^2 + W$, where the effective potential energy W is given by

$$W(q, q_m, u) = -\frac{3\beta q^2(q_m^2 - q^2)}{(1 + 9\beta q^2 + u^2)(1 + 3\beta q^2 + u^2)}\left[3\beta q^2 + 1 - \frac{u^2}{1 + 3\beta q_m^2}\right]. \tag{56}$$

An analysis of the expression in square brackets shows that if the speed of the breather is not too high,

$$|u| < (1 + 3\beta q_m^2)^{1/2} \tag{57}$$

the effective potential energy is negative at $0 \le q \le q_m$ and graphs of $W(q)$ are similar to the curve shown in Fig. 3 for the case $C_1 = 0$. Solving for q' from (54) and integrating over ξ yields the breather amplitude $q(\xi)$ which looks similar to the profile of the standing breather (29). If the inequality (57) is not satisfied, then the effective potential energy (56) becomes positive in some vicinity of $q = 0$, when $(1 + 3\beta q_m^2)^{1/2} < u < 1 + 3\beta q_m^2$; it is positive along the entire interval $0 < q < q_m$, when $1 + 3\beta q_m^2 < u$. In both cases there are no trajectories corresponding to breather-like solutions, so Eq. (57) is a necessary and sufficient condition for the existence of a moving breather with arbitrary amplitude.

The new solution represents a generalization of the previous solution (43) to the case of high amplitude breathers. The important result is the dependence of k on x and t described by (53). The wave vector $k = \phi'$ has approximately

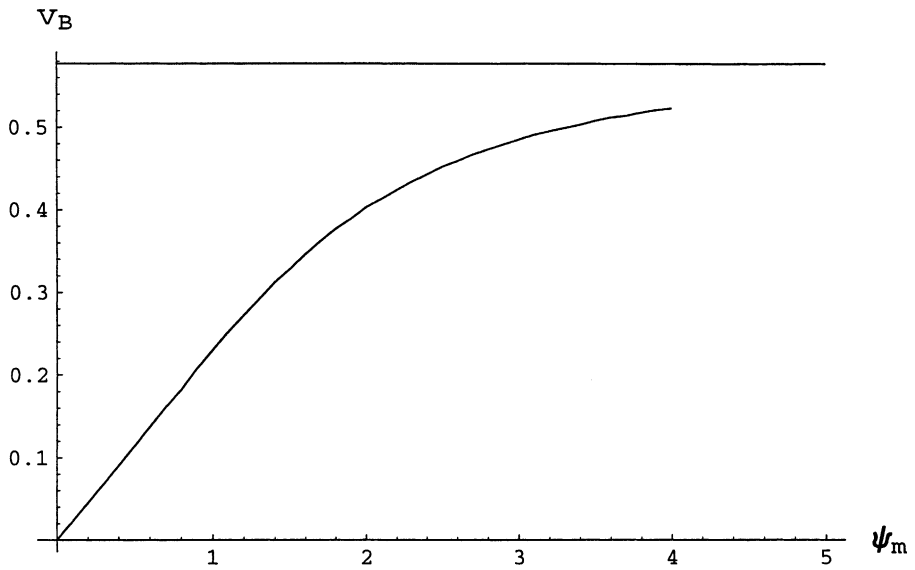

Fig. 7. Dependence of the breather velocity v_B on its amplitude ψ_m, obtained from the virial theorem. The horizontal line shows asymptotic value of v_B and $\psi_m \to \infty$.

the same value as given by (44) in the tail zone of the breather and sharply decreases near the peak dropping down to $2u/3\beta q_m^2$. Although the new solution is an exact solution to the full a^2-order equation (13), the value of velocity is a free parameter with some weak restriction (57). Similar to the calculation of v_B in the small amplitude case (45), we make use of the virial theorem based on (41) to estimate the effect of large amplitudes on breather velocity. Expressing Ψ and Ψ^* in (39) in terms of $q(\xi)$ and $\phi(\xi)$ and substituting into (41) gives a Hamiltonian density as a function of $q(\xi)$ and $k(\xi) \equiv \phi'(\xi)$

$$H(q_m, u, \xi) = -\tfrac{1}{2}k^2q^2(1 + 3\beta q^2) - \tfrac{1}{2}q'^2(1 + 9\beta q^2) + 3\beta q^4. \tag{58}$$

It is possible to evaluate the first integral in (42) and formulate the virial theorem, $\mathcal{H}(q_m, u) = 0$, by using the identity $\mathcal{H} = \int H \, \mathrm{d}\xi \equiv \int H \, \mathrm{d}q/q'$. The result after some algebra and a numerical integration over $\mathrm{d}q$ gives the velocity $u \equiv v_B$ as shown in Fig. 7. For low amplitude, the velocity is in agreement with (45) obtained with the use of (43), while for high amplitude we see that v_B becomes asymptotically constant. The remaining quantities that are required to obtain the scaling (38) at high amplitude are obtained in a straightforward way. Taking the wavenumber of the fastest growing large amplitude mode, from (37), we find that $n_B \propto k_{max} = \text{const.}$, independent of ψ_m, which is consistent with the asymptotic assumption of $v_B = \text{const.}$ if we admit the above mentioned relationship between k and k_m. From the asymptotic large amplitude expansion of I, in (33), we have $\psi_m \propto E^{1/4}$ (with n independent of ψ_m and roughly half the energy in the proto-breathers). Performing the integration in (47) for the high amplitude case when the width of the breather $d \simeq 5 = \text{const.}$, we find

$$\sigma \propto \psi_m^4 \propto E. \tag{59}$$

Combining the results of v_B and n_B independent of initial E, with (59), in (38), this gives, at the start of the coalescence, that $\tau_B \propto E^{-1}$. We must, however, follow the time evolution of the coalescence process until a single breather is formed. To do this we note that the time constant is governed by $n_B^{-1}(\mathrm{d}n_B/\mathrm{d}t) = n_B\sigma v_B$, since n_B decreases as E_B^{-1} and σ increases as E_B, i.e., if the total energy in the breathers remains nearly constant, then

$n_B\sigma$ = const. during the coalescence. As found numerically (see below) v_B is relatively constant during this process, and thus we conclude that $n_B^{-1}(dn_B/dt) = 1/\tau$, a constant, during the decay. Thus the final proportionality for the scaling of coalescence, assuming $E_B \propto E$, is

$$\tau_B \propto E^{-1}, \tag{60}$$

which agrees with the numerical coalescence time.

5.2. Numerical results

We perform numerical calculations on the discrete oscillator chain to check the approximations and also account for discreteness effects. We first enquire if the decay is characterized by a single time constant, i.e., if the total number of breathers N_B obeys $(1/N_B)(dN_B/dt) = 1/\tau$, a constant. Taking typical cases of initial energy $E = 20, 50$ in mode $\gamma = 120$, we plot $\ln N_B$ versus t, in Fig. 8a and b, respectively. The resulting decays are straight line, indicating the constancy of τ.

This constancy of τ in the decay process was found to hold well for initial energies $20 \leq E \leq 100$, which is a typical intermediate energy range. Using results like those in Fig. 8a and b the results in Fig. 9 are obtained, in the range $20 \leq E \leq 250$. A straight line gives a power law fit to the coalescence time τ_B versus energy, with a best fit giving $\tau_B \propto E^{-1.12}$. This is almost the same as the scaling of $\tau_B \propto E^{-1.19}$ in [19] using a somewhat more qualitative criterion for τ_B. Note that τ_B is not the same as the time constant τ. Typically, there are 8–9 initial proto-breathers which coalescence, with the time τ_B being the time necessary for a single chaotic breather to be established. Since in all cases the initial conditions have most of the energy in mode 120, the 8–9 initial peaks tends to be a strong initializing effect for the proto-breathers, as already mentioned in Section 4.

A further confirmation of our picture of the coalescence process is seen in Fig. 10 and 11. In Fig. 10, for the case of $E = 20$, the motion of the largest peak is followed. During the initial stage of proto-breather formation, the motion is not well defined as early unstable motion and collisions do not conserve a single proto-breather having the maximum amplitude. At time of 10^4 s the largest breather is established and grows in energy with associated increasing velocity. The velocity at relatively large amplitude then remains fairly constant in the range 2×10^4 s $\leq t \leq 4 \times 10^4$ s, after which time Fig. 8a indicates the existence of a single dominant breather. As seen in Fig. 11, the energy of the largest breather continues to grow, statistically, during this time. For 4×10^4 s $\leq t \leq 10^5$ s, in Fig. 10 the single chaotic breather gradually slows down in a somewhat uneven fashion. The explanation of this effect is not within the envelope theory but can be quantitatively understood by two effects, the well-known pinning effect due to the discreteness [18], and the continual interaction with background modes containing a total energy of the order of the breather energy. As seen in Fig. 11, during this period the main breather energy is growing slightly. The breather is taking energy from high-frequency modes with similar symmetry and giving energy to low-frequency modes that do not have this symmetry. As described previously [19] and will also be developed in Section 6, the breather will decay at longer times, as energy continues to be transferred to low-frequency modes and equipartition is approached. Similar dynamics occurs at higher energies, but more rapidly so that the phenomena are not as clearly observed.

6. Breather decay

In the usual picture of breather stability, the physical mechanism by which the breather loses stability is that the breather frequency becomes resonant with a linear normal mode [15,16,27]. This explanation is not directly applicable to our problem as the breather frequency is higher than the highest mode; e.g., for $E = 50$ ($\beta = 0.1$,

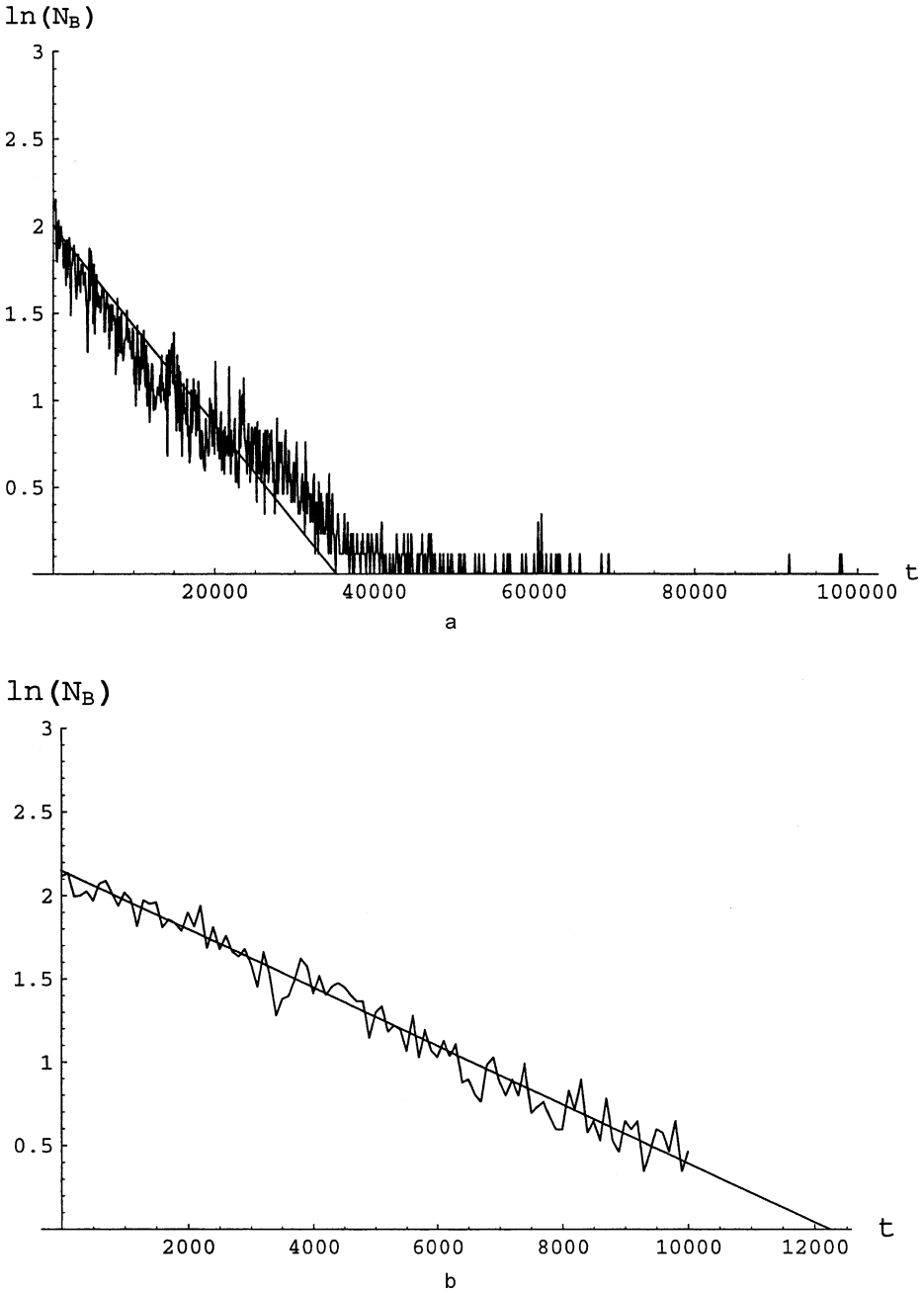

Fig. 8. Numerical dependences of the number of breathers, $\ln N_{\mathrm{B}}(t)$, versus time. The straight line curves indicate the constancy of the decay time τ during the coalescence from 8–12 breathers to two breathers. The final coalescence to one breather has less statistical accuracy. (a) Initial energy $E = 20$, $n = 9$. (b) Initial energy $E = 50$, $n = 9$.

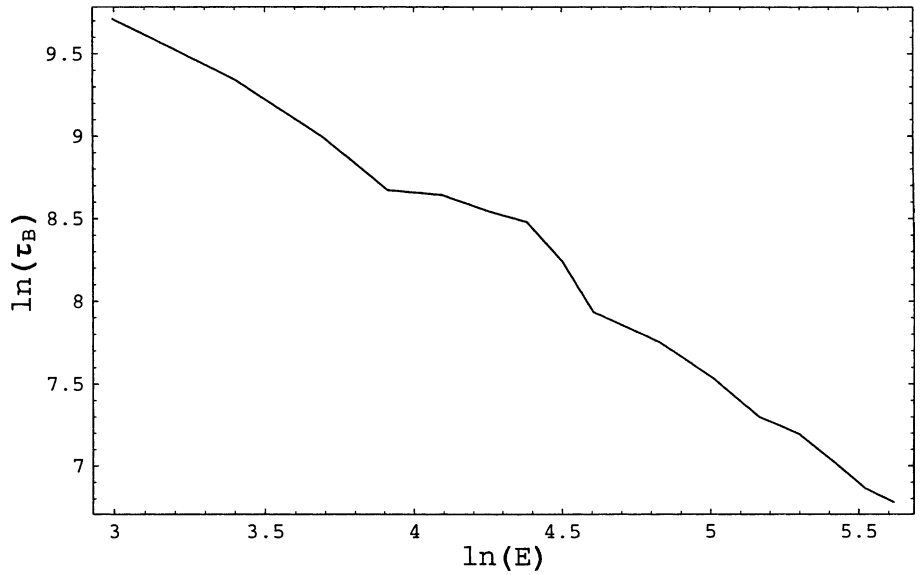

Fig. 9. Numerical results illustrating the dependence of the decay time $\ln \tau_B$ versus initial energy $\ln E$ obtained from results at various energies as described in Fig. 8.

$N = 128$), the CB has a frequency $\omega_B = 2.62$ while the highest mode frequency is $\Omega_h \simeq 2$. However, we know this breather is not completely stable (a CB), as it was formed in the chaotic portion of the Hamiltonian phase space. Within the usual theory, the process then becomes quite subtle, as it depends on the relatively small continuous spectrum of the chaos.

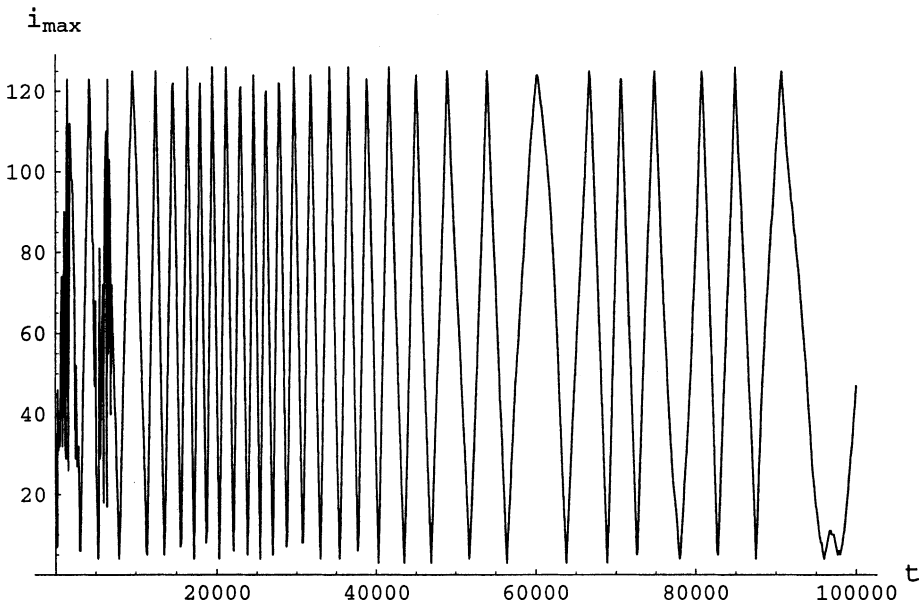

Fig. 10. Time dependence of the oscillator number i_{max} defined as the position of the oscillator having a maximum energy in comparison with all other oscillators at a given time t. After 10^4 s, when a largest breather is established, it shows the position of that breather.

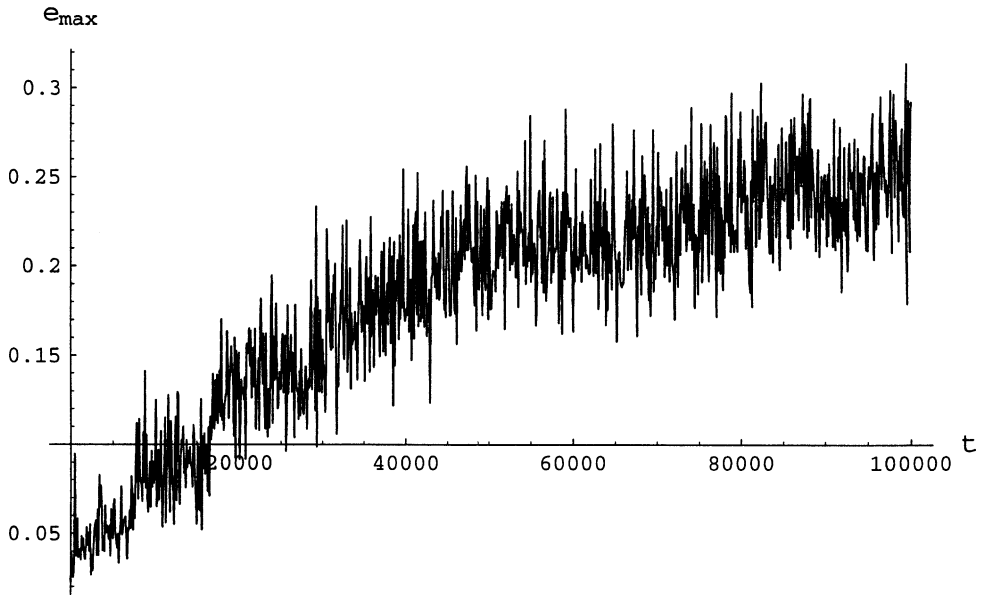

Fig. 11. Time dependence of the maximum energy $e_{i_{\max}}$ of the oscillators described in Fig. 10. After the largest breather is established it corresponds to the energy of the oscillator at the peak of the breather.

Although the dominant structure is the CB, the mode spectrum, in which the CB can be decomposed, plays an important role. For energy transfer from low-frequency to high-frequency modes, it was shown that the stochasticity developed in low-frequency beat oscillations could transfer energy to the high-frequency modes via the Arnold diffusion mechanism. The key requirement for energy transfer on a time scale that is not exponentially slow is that the beat oscillation frequency be as high or higher than the mode (or beat mode) to which the energy is being transferred [9]. In a subsequent paper [20], the scaling $T_{\rm eq}$ (low to high) $\propto (E/N)^{-3}$ was predicted and confirmed numerically. In [19], we used the same formalism to predict the scaling $T_{\rm eq}$ (high to low) $\propto (E/N)^{-2}$, which we found numerically. However, the predicted estimate of the time to equipartition was nearly 2 orders of magnitude shorter than the numerical result. Our current study of breather dynamics has revealed that the method was not applied correctly in [19] when the dominant dynamics is the breather, rather than the normal modes. Re-examining the beats in the high-frequency normal modes indicates that the beat frequency is

$$\Omega_{\rm B} = \omega_{\rm B} - \Omega_{\rm h}, \tag{61}$$

i.e., the difference between the frequency locked to the breather and the background-free normal modes. The interaction is with the high-frequency normal modes so we take $\Omega_{\rm h} \simeq 2$. For $E = 50$ with $\omega_{\rm B} = 2.62$, we find, in Fig. 12, the dominant beat frequency $\Omega_{\rm B} \simeq 0.6$, which is close to the value $\Omega_{\rm B} \simeq 0.62$ given by (61).

The key assumption in the calculation is to require, for fast Arnold diffusion [9], that

$$\Omega_{\rm B} \geq \delta\Omega_l = \frac{\pi\,\delta l}{N}, \tag{62}$$

where δl is the number of low-frequency modes to which energy can be transferred, which are taken to correspond one-to-one with high-frequency modes, δk, $\delta l = \delta k$. To estimate the energy transfer, we transform the Hamiltonian

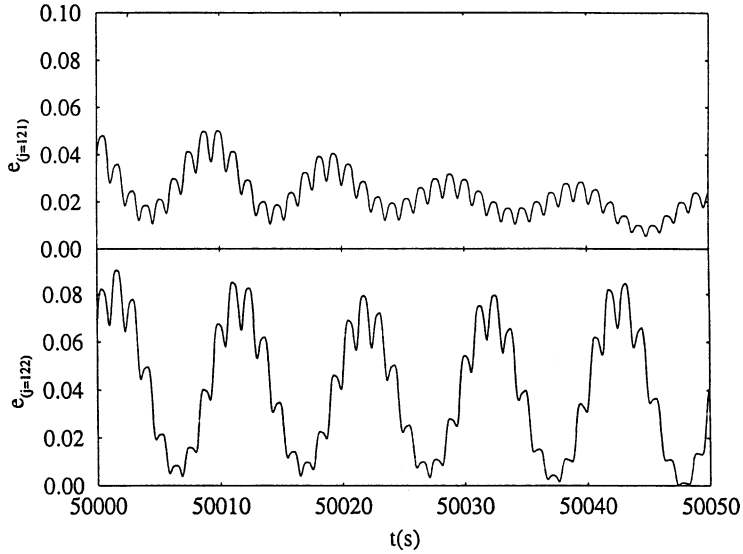

Fig. 12. Time dependence of the energy of normal mode E_j for $j = 121$ and 122 during the time interval 50 000 s $< t <$ 50 050 s when a single chaotic breather is well established ($E = 50$, $n = 9$).

(1) to normal modes, using (6) and (7), and then introducing the canonical action–angle variables (I, ϕ) through the transformation $Q_j = \sqrt{2I_j/\Omega_j}\cos\phi_j$ and $P_j = \sqrt{2I_j\Omega_j}\sin\phi_j$, we obtain [9]

$$H = \sum_j \Omega_j I_j + \left(\frac{\beta}{8N+8}\right) \sum_{i,j,k,l} G(i,j,k,l)\sqrt{\Omega_i\Omega_j\Omega_k\Omega_l I_i I_j I_k I_l}\,\mathrm{ang}(ijkl), \tag{63}$$

where $\mathrm{ang}(ijkl) \equiv \cos\phi_i \cos\phi_j \cos\phi_k \cos\phi_l$. The coefficients G, as calculated in [3,9] are

$$G(i,j,k,l) = \sum_P B(i+j+k+l), \tag{64}$$

where P represents the eight permutations of sign of j, k and l and the function $B(x)$ takes the value 1 if the argument is zero, -1 if the argument is $\pm 2(N+1)$, and zero otherwise. The selection rule (64) follows from the quartic nature of the coupling. Taking the derivative of H with respect to a high-frequency angle, we obtain energy transfer from any high-frequency mode to all accessible low-frequency modes in the form

$$\frac{\mathrm{d}E_j}{\mathrm{d}t} \simeq C_j\Omega_j\left(\frac{\beta}{N}\right) C_l\delta l E_j E_l. \tag{65}$$

The quantity $C_l\delta l$ is reduced from the quartic sum by the following. The derivative reduces the sum by one index, and the selection rule (64) by a second index, so the sum runs over some $(\delta l)^2$ modes. Assuming every quartic term in this sum is typically of the same size and taking the phases to be random, then the effective number of terms is $C_l\delta l$, where C_l was estimated in [20] to be $C_l = \frac{1}{4}$. The quantity C_j is an efficiency of energy transfer by the Arnold diffusion mechanism, which must be less than $\frac{1}{2}$ (see [1]) and we take $C_j = \frac{1}{4}$ for definiteness. Note that both factor C_l and C_j were omitted in [19] which contributed to the underestimation of the equipartition time in that paper. However, our main reworking of that calculation is a new determination of δl from (62) using Ω_B from (61).

From (32), we calculate $E_\mathrm{B}(\psi_m)$ and from (21) we approximate ω_B, both for $n = 1$ (a single breather). From these results, and using (61) we obtain a graph of $\Omega_\mathrm{B}(E_\mathrm{B})$ as given in Fig. 13 on log–log scale, which we compare

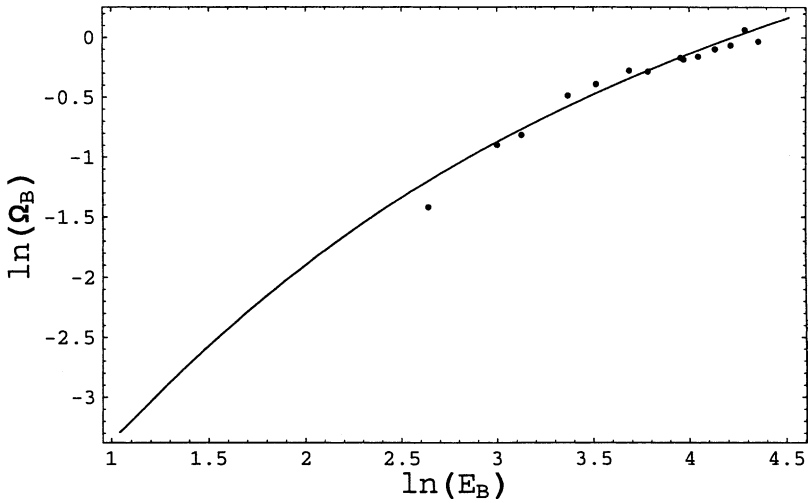

Fig. 13. Theoretical curve and numerical points illustrate the dependence of beat frequency, $\ln \Omega_{\mathrm{B}}$, on energy, $\ln E_{\mathrm{B}}$, indicating a nearly linear proportionality in the energy range investigated.

with numerical results for Ω_{B}. We see that over the main range of energies investigated, we find, approximately, $\Omega_{\mathrm{B}} \propto E_{\mathrm{B}}$ (slope of unity) and furthermore we have an approximate value $\Omega_{\mathrm{B}} \simeq 0.2\beta E_{\mathrm{B}}$. Substituting this, in (62), with the equality, we have

$$\delta l = \frac{N}{\pi} \times 0.2\beta E_{\mathrm{B}}. \tag{66}$$

Since, within our approximation, $\mathrm{d}E_j/E_j = \mathrm{d}E_{\mathrm{B}}/E_{\mathrm{B}}$, (65) can be rewritten as

$$\frac{\mathrm{d}E_{\mathrm{B}}}{E_{\mathrm{B}}^2} = -0.2\beta C_j C_l \Omega_j \frac{\beta}{N}\frac{N}{\pi} E_l \,\mathrm{d}t. \tag{67}$$

As in previous work, we integrate from E_{B} (initial) to Ed/N, where $d = n_b^{(\mathrm{init})}$ is the initial number of oscillators in the breather, and E_l is integrated from zero to E/N. Using the simplest assumption that $E_l(t) = (t/T_{\mathrm{eq}})E/N$, a diffusive process, and taking $d \simeq 5$, we obtain

$$T_{\mathrm{eq}} \simeq \frac{80\pi}{5}\left(\frac{N}{\beta E}\right)^2, \tag{68}$$

where we have substituted $C_j = C_l = \frac{1}{4}$ and $\Omega_j = 2$. We have obtained the scaling $T_{\mathrm{eq}} \propto \epsilon^{-2}$, as found numerically in [19]. For $\beta = 0.1$, $N = 128$ and $E = 50$, $T_{\mathrm{eq}} \simeq 3.3 \times 10^4$. This is about a factor of 5 shorter than the time of $T_{\mathrm{eq}} \simeq 1.6 \times 10^5$ s reported in [19].

There are various arguments to conclude that we have somewhat underestimated the time to equipartition. Particularly, we have not explicitly considered the complicated process, at intermediate times when the principle CB has been formed but not decayed, and is transferring energy from high-frequency modes that are not part of the breather, to low-frequency modes, using the breather as a catalyst for the transfer. To see these effects we repeat, in a slightly different form from [19], computations of n_{osc} and n_{eff}, given in Fig. 14a and b, for $E = 50$, over a time scale in which the various longer time scale dynamical processes can be seen. The coalescence time period is seen for $t < 2 \times 10^4$ s during which n_{osc} is decreasing rapidly. This is followed by a period ($\Delta t \sim 10^5$ s) in which

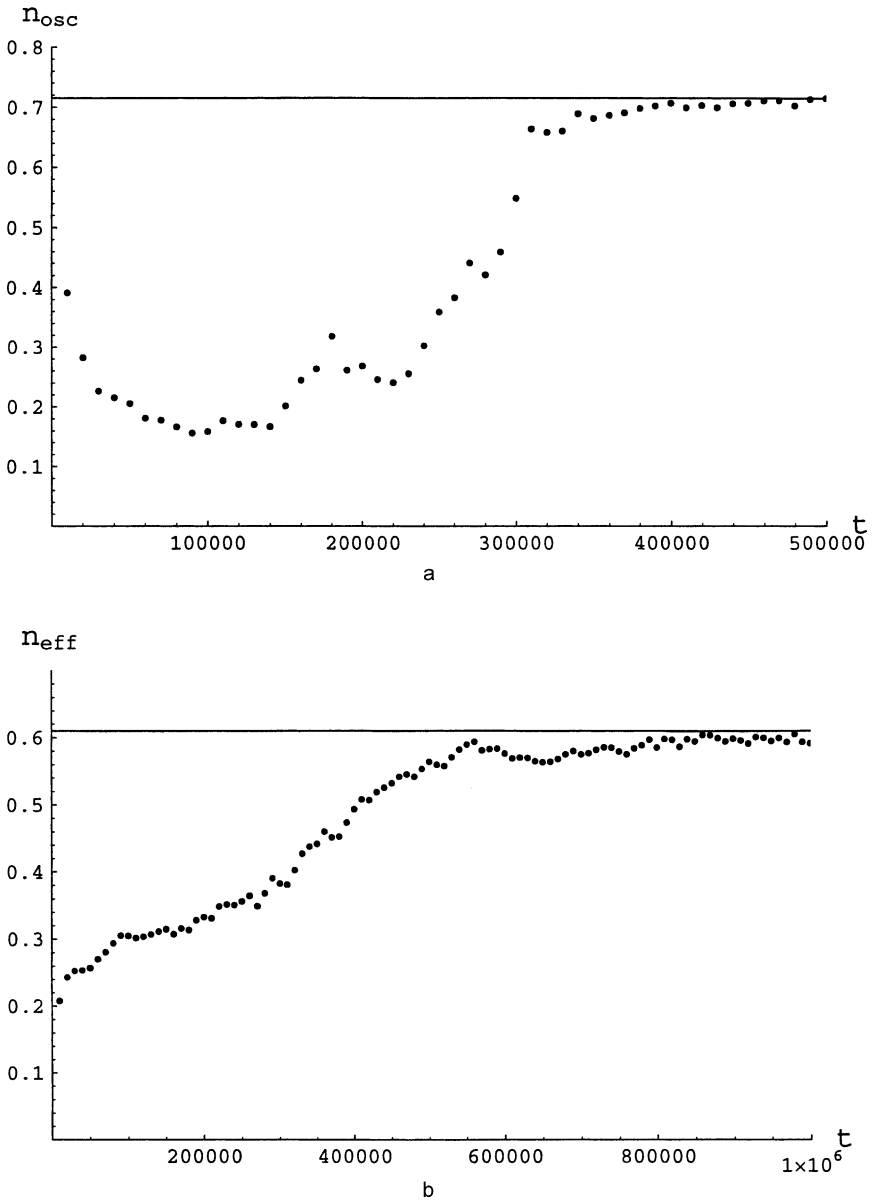

Fig. 14. Time dependence of: (a) $n_{\mathrm{osc}}(t)$, and (b) $n_{\mathrm{eff}}(t)$. The horizontal lines are theoretical asymptotes.

a single breather is first increasing and then decreasing slowly as energy is transferred from high-frequency modes to low-frequency modes. Finally, there is the larger increase in n_{osc}, during which time the breather energy decays, until equipartition is reached at roughly the time $t \simeq 3 \times 10^5$ s. An average over 10 initial conditions gave the value of $T_{\mathrm{eq}} \simeq 1.6 \times 10^5$ s, reported in [19]. The equipartition level at $n_{\mathrm{osc}} \simeq 0.7$ and $n_{\mathrm{eff}} \simeq 0.6$ can be explained by fluctuations, as described in [12,18]. There are some subtitles, not reported in those references, which we describe in Appendix D. We have continued the numerical calculation to $t = 10^7$ s and find the equipartition values to be maintained very closely.

7. Conclusions

The FPU-β chain of equal masses coupled to nearest neighbors by hard springs with quartic nonlinearity has a very interesting dynamics, with quite different behavior depending on whether the energy is initially in the low- or high-frequency part of the spectrum. Most investigations have taken the initial conditions in a low-frequency linear mode or modes for which neighboring oscillators are mostly in phase. The process by which a resonant interaction of a few low-frequency modes can lead to stochastic beat oscillations, that diffusively transfer energy to high-frequency modes, has been well studied.

In contrast, if the energy is placed in a high-frequency mode or modes, for which neighboring oscillators are primarily out of phase, a more complicated dynamics ensues. High-frequency mode initial conditions have phase symmetry of neighboring oscillators close to that of a localized exact breather, but have a different amplitude profile. The resulting dynamics consists of three stages. First, there is an initial stage in which the mode breaks up into a number of breather-like structures. Second, on a slower time scale, these structures coalesce into one large unstable structure, called a CB. Since a single large CB closely approximates a stable breather, the final decay stage, toward equipartition, can be very slow.

Considerable insight into the behavior of a nonlinear oscillator chain, starting from high-frequency initial conditions, can be obtained by introducing an envelope function for the displacements of the oscillators. The initial conditions for the envelope only contain significant long wavelength perturbations. For the envelope function an expansion is then possible to obtain a nonlinear PDE which approximates the behavior of the discrete system.

For the quartic FPU chain with fixed ends, Taylor expanded to fourth-order in the separation between oscillators, we have obtained PDEs approximating the envelope function of the discrete chain. The resulting equations have been solved to obtain nonlinear periodic structures similar to isolated breather solutions, showing that the width decreases with the amplitude at low amplitude and becomes asymptotically constant at high amplitude, analogous to the behavior of isolated stable breathers.

We have numerically examined the relaxation of the initial conditions toward equilibria. Underlying stability considerations, and the proximity of equilibria with other symmetries, lead to breakup of the initial symmetry, if the energy is sufficiently high. The number of chaotic breathers established in this process, starting from a symmetry of a few initial peaks, is usually larger than the initial number of peaks, but depends on the energy. The particular case studied in [19], and also in this paper, of $n = 9(\gamma = 120)$ led to results of 8–12 proto-breathers in the energy range $20 < E < 200$. This result can be qualitatively understood by a balance between a minimizing of the oscillation amplitude within a peak with a tendency for the peaks to remain isolated.

After a set of CBs are formed, they move slowly in random directions, colliding with one another, and losing or gaining energy in the interaction. On an average, the large structures absorb energy from the smaller ones, as expected from general theoretical considerations. The time constant for coalescence into a single CB was estimated in [22] from the relation $\tau_B \simeq (N_B \sigma v_B)^{-1}$, where N_B is the breather number, σ a collision cross-section for absorption, and v_B a characteristic velocity. Using this procedure, extended to higher energies, we obtained reasonable agreement with the numerical scalings of $\tau_B \propto E^{-1}$. Furthermore, we demonstrated that $\tau \equiv N_B(\mathrm{d}N_B/\mathrm{d}t)^{-1}$ is essentially constant during the decay, such that $\tau_B \propto \tau$, in agreement with our theoretical prediction.

To calculate the scaling and the time T_{eq} to obtain energy equipartition, we adopted a theory developed for stochastic transfer of energy from low-frequency to high-frequency modes by means of chaotic beat oscillations [20]. We predict that $T_{eq} \propto \epsilon^{-2}$, as found numerically, for varying E and constant N, and furthermore were able to calculate a value of T_{eq} for $E = 50$ to within a factor of 5 of the numerical value. The numerical equipartition values of $n_{osc} \simeq 0.7$ and $n_{eff} \simeq 0.6$, for oscillators and modes, respectively, agreed with analytic values.

We conclude that the process, by which the energy initially placed in a high-frequency mode reaches equipartition among modes, is understood. The time scales for the longer time processes can also be calculated approximately.

The physical mechanism explains why the transfer of energy from high- to low-frequency modes is slower than the reverse transfer. It also sheds light on the interesting question of whether nonlinear chaotic process will tend to create coherent localized structures. The answer, at least within the context of this study, is that such localized structures can form transiently, but the ultimate most probable state is that of equipartition among the system modes.

Acknowledgements

This work was partially supported by the National Science Foundation Grant PHY-9729668. We thank Dr. Kai Ullmann for use of his numerical code.

Appendix A. Asymptotic expansion of $I(y)$

Expressing (24) in terms of $y = 6\beta\psi_m^2$ and making straightforward transformations yields

$$I(r, y) = \frac{2}{\pi}\int_0^{\pi/2} \frac{\mathrm{d}\alpha}{\sqrt{\sin^2\alpha + r^2}} + \frac{18y}{\pi}\int_0^{\pi/2} \frac{\mathrm{d}\alpha \sin^2\alpha}{\sqrt{\sin^2\alpha + r^2}} \frac{1}{(\sqrt{1 + 9y\sin^2\alpha} + 1)}. \tag{A.1}$$

Applying an asymptotic expansion at $r \to 0$ for the first integral and putting $r = 0$ in the second one gives

$$I(r, y) = \frac{2}{\pi}\ln\frac{4}{r} + \frac{18y}{\pi}\int_0^{\pi/2} \frac{\mathrm{d}\alpha \sin\alpha}{\sqrt{1 + 9y\sin^2\alpha} + 1}. \tag{A.2}$$

After a few substitutions, the integral is calculated analytically yielding an asymptotic expression for $I(r, y)$,

$$I(r, y) = \frac{2}{\pi}\ln\frac{4}{r} + \frac{6\sqrt{y}}{\pi}\arcsin\sqrt{\frac{9y}{9y+1}} - \frac{1}{\pi}\ln(9y + 1). \tag{A.3}$$

Appendix B. Energy of the nonlinear envelope solutions

Expression (1) for energy H can be rewritten in terms of envelope function $\psi_i(t) = (-1)^i q_i(t)$:

$$H = \sum_{i=0}^{N+1}\left[\frac{1}{2}\dot{\psi}_i^2 + \psi_i^2 + \psi_{i+1}\psi_i + \frac{\beta}{2}(\psi_i^4 + 3\psi_{i+1}^2\psi_i^2 + 2\psi_{i+1}^3\psi_i + 2\psi_{i+1}\psi_i^3)\right]. \tag{B.1}$$

Substituting Taylor's expansion (12) and collecting terms proportional to different powers of a up to a^2 yields

$$H = \frac{1}{a}\int_0^{(N+1)a} \mathrm{d}x \left\{\frac{1}{2}\psi_t^2 + 2\psi^2 + 4\beta\psi^4 + a(\psi\psi_x + 7\beta\psi^3\psi_x) + \frac{a^2}{2}[\psi\psi_{xx} + \beta(7\psi^3\psi_{xx} + 9\psi^2\psi_x^2)]\right\}. \tag{B.2}$$

Introducing the dimensionless variable $x \to x/a$, performing an integration by parts and taking into account boundary conditions $\psi(0, t) = \psi(N + 1, t) = 0$ yields

$$H = \frac{1}{12}[\psi_x^2(0) - \psi_x^2(N + 1)] + \int_0^{N+1} \mathrm{d}x \left(\frac{1}{2}\psi_t^2 + 2\psi^2 + 4\beta\psi^4 - \frac{1}{2}\psi_x^2 - 6\beta\psi^2\psi_x^2\right). \tag{B.3}$$

Applying this expression for the harmonic dependence $\psi(x,t) = \psi(x)\cos\omega t$ and averaging over time with $\cos^2\omega t = \frac{1}{2}$, $\cos^4\omega t = \frac{3}{8}$ gives

$$H = \frac{1}{24}[\psi_x^2(0) - \psi_x^2(N+1)] + \frac{1}{4}\int_0^{N+1} \mathrm{d}x(\omega^2\psi^2 + 4\psi^2 - \psi_x^2 + 6\beta\psi^4 - 9\beta\psi^2\psi_x^2). \tag{B.4}$$

Substituting (28) into (B.4) yields Eq. (32) for the energy of the system. For the case of a strongly nonlinear envelope, putting $r = 0$, allows us to express energy as

$$E = \left(\frac{2n\psi_m}{\sqrt{6\beta}}\right) Z(y), \tag{B.5}$$

where $y = \beta\psi_m^2$ and

$$Z(y) = \int_0^{\pi/2} \mathrm{d}\alpha(1 + 9\beta\psi_m^2\sin^2\alpha)^{1/2}(3\beta\psi_m^2\sin^3\alpha + 2\sin\alpha). \tag{B.6}$$

The integral $Z(y)$ is calculated exactly, giving

$$Z(y) = \frac{25}{24} + \frac{9}{8}y + (23 + 234y + 243y^2)\frac{\arctan(3\sqrt{y})}{72\sqrt{y}}. \tag{B.7}$$

Appendix C. Conditions of validity of a^2-approximation

Analytic results in Section 3 are based on the reduced form (18) in which all terms proportional to a^4 and higher powers of a are dropped. We now examine their accuracy numerically solving (14) which includes all terms of order a^4. Comparing linear terms, one concludes that the reduced linear form of (14) has one additional term, $\frac{1}{12}\psi_{xxxx}$, with respect to (15). Its solutions with zero boundary conditions at $x = 0$ and $N + 1$ have eigenfrequencies

$$\omega^2 = 4 - q_n^2 + \tfrac{1}{12}q_n^4, \quad q_n = \frac{\pi n}{(N+1)} \tag{C.1}$$

higher by the factor $\frac{1}{12}q_n^4$ than given by (17).

The nonlinear equation (14) has an exact first integral which can be obtained by multiplying by ψ_x and integrating over x giving

$$(-\omega^2 + 4)\psi^2 + (1 + 9\beta\psi^2)(\psi_x^2 + \tfrac{1}{6}\psi_x\psi_{xxx} - \tfrac{1}{12}\psi_{xx}^2) + \beta(6\psi^4 + 3\psi\psi_x^2\psi_{xx} + \tfrac{3}{8}\psi_x^4) = C_1. \tag{C.2}$$

Choosing, $C_1 = 0$, we select the class of localized, breather-like solutions for a chain of oscillators that is infinitely long ($N \to \infty$). The breather envelope function has one maximum, ψ_m, and $\psi \to 0$ at $x \to \pm\infty$. Applying (C.2) at $x = 0$, with $\psi_x(0) = 0$, $\psi_{xx}(0) < 0$, yields an equation for the eigenfrequency

$$\omega^2 = 4 + 6\beta\psi_m^2 - \tfrac{1}{12}(1 + 9\beta\psi_m^2)f_{xx}(0)^2, \tag{C.3}$$

where $f(x)$ is the normalized $\psi(x)$. The result is that breather frequency, calculated from (14) to order a^4, is less than the value in (21), to order a^2. Note that for linear modes (C.1) the a^4 term causes an increased frequency. Substituting (C.3) into (C.2), the factor $f_{xx}(0)$ plays the role of an eigenvalue, which is found numerically by applying the shooting method to (C.2) with the boundary conditions, $\psi(\pm\infty) = 0$, $\psi_x(0) = 0$. The constraints are applied at some distant points $\pm x_0$, which is possible due to the existence of analytic asymptotic solutions at

$x \to \pm\infty$, where $\psi(x) \to 0$ and, correspondingly, all β-dependent terms in (C.2) can be omitted. This leads to the exponential profile for the breather tail

$$\psi(x) \to C\exp(-\kappa|x|), \quad x \to \pm\infty, \tag{C.4}$$

where the rate of decay, κ, is determined by substitution of exponentially small (C.4) into Eq. (C.2) with β-terms neglected, obtaining

$$\kappa^2 = \sqrt{36 + 72\beta\psi_m^2 - f_{xx}(0)(1 + 9\beta\psi_m^2)} - 6. \tag{C.5}$$

Expression (C.5) is valid if $(1 + 9\beta\psi_m^2) f_{xx}^2(0) < 72\beta\psi_m^2$.

Substituting the infinite Taylor's series (12) into the linearized equation (2) and assuming an exponential law of decay (C.4) yields a universal relation

$$\omega = 2\cosh\frac{\kappa}{2}, \tag{C.6}$$

which is an exact result.

The factor $f_{xx}(0)$ is used to estimate the half-width of the bulk envelope function as $\Delta \simeq |f_{xx}(0)|^{-1/2}$, while κ^{-1} describes the half-width of the tail. From analytic results for a breather, derived from Eq. (18), we obtained

$$f_{xx}(0) = -\frac{6\beta\psi_m^2}{1 + 9\beta\psi_m^2}. \tag{C.7}$$

As is seen from both (C.6) and (15) in the a^2-approximation, $\kappa^{-1} = (6\beta\psi_m^2)^{-1/2}$. The factor Δ, calculated from (C.7), equals κ^{-1} in the small amplitude limit and becomes large, $\Delta = (\frac{3}{2})^{1/2}$, in the strongly nonlinear regime, indicating that, for large amplitude, the breather envelope function has a two-scale structure. Numerical integration of (C.2) is presented in Fig. 15, illustrating dependencies of ω, Δ and κ^{-1} on ψ_m in both a^2 (dashed line) and a^4 (solid line) approximations. The breather profiles described by (29) thin line, (32) dashed line, in a^2-approximations and the a^4 results based on numerical integration of (C.2) are illustrated in Fig. 16 for a few typical values of ψ_m. Figs. 15 and 16 show that there is no significant difference between the a^2 and a^4 approximations up to $\psi_m \simeq 2$; a limit of applicability of Eq. (18) and the solution in (29). Analytical small amplitude approximation (30) is in a good agreement with the numerical curves at lower amplitudes, $\psi_m \leq 0.5$.

Appendix D. Asymptotic values of n_{eff} and n_{osc} in equipartition

The effective number of normal modes containing energy is defined by

$$n_{\text{eff}} = \frac{1}{N}\exp\left[-\sum_{j=1}^{j=N} e_j \ln e_j\right], \tag{D.1}$$

where $e_j = E_j/E_{\text{h}}$ are the normalized linear energies of the normal modes

$$E_j = \Omega_j(Q_j^2 + P_j^2), \tag{D.2}$$

where $E_{\text{h}}{=}\sum_1^N E_j$ given by (5). Only the quadratic terms in the potential energy are taken into account in (D.2) so

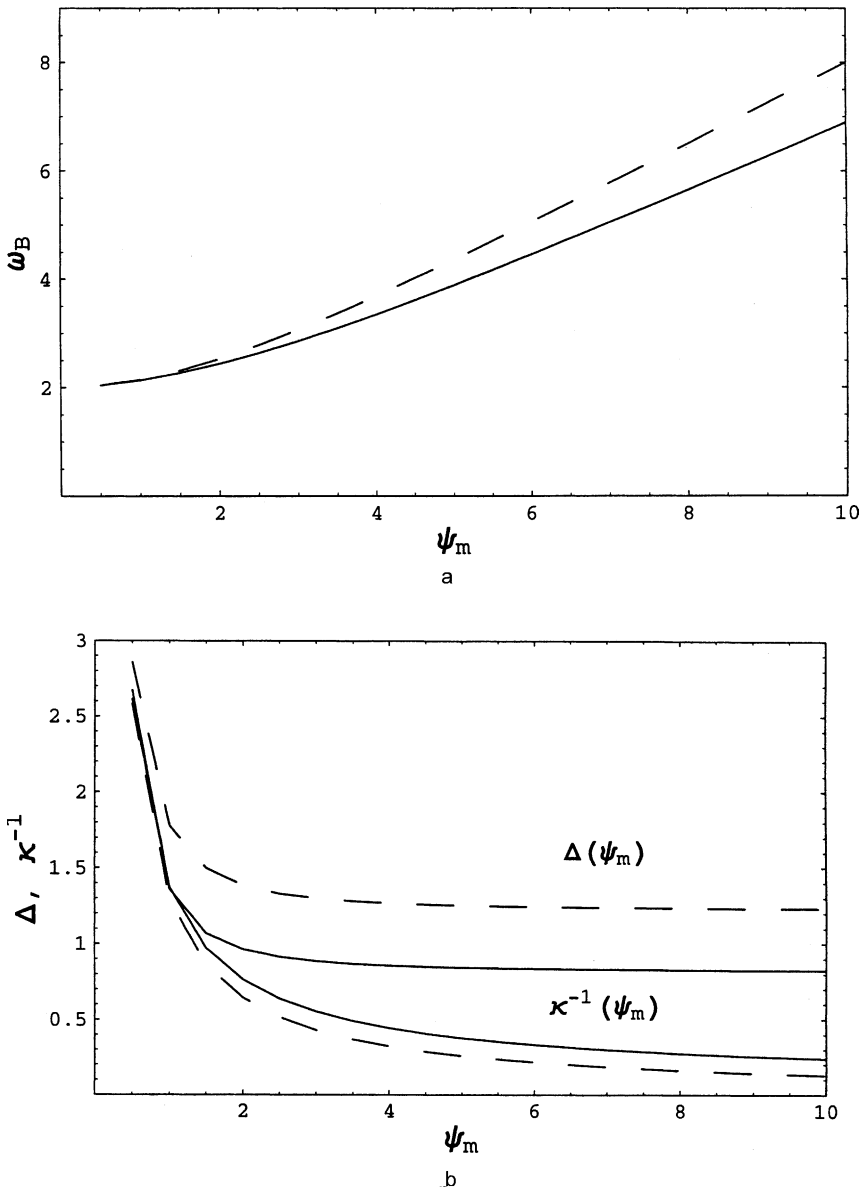

Fig. 15. Dependences of (a) ω_B, and (b) Δ and κ^{-1} on breather amplitude, ψ_m; the solid curves correspond to a^4-approximation, the dashed curves to a^2 approximations.

that E_h is not the total energy E and not exactly conserved during the relaxation. The effective number of oscillators containing energy

$$n_{osc} = \frac{1}{N}\exp\left[-\sum_{i=1}^{i=N} e_i \ln e_i\right] \tag{D.3}$$

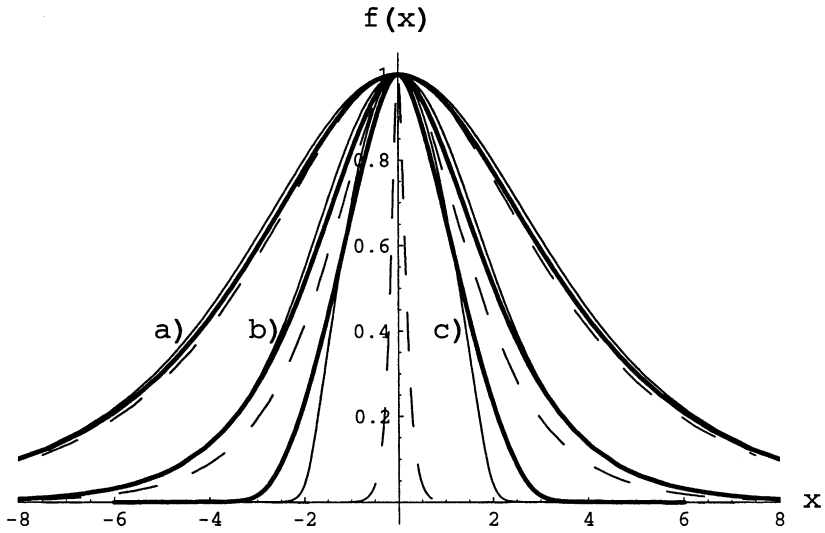

Fig. 16. Comparison of the breather profiles obtained in a^2-approximation (Eq. (29), thin solid curves); (Eq. (30), dashed curves) and in a^4-approximation (Eq. (14), thick solid curves) for three values of the amplitudes; (a) $\psi_m = 0.5$, (b) $\psi_m = 1$, (c) $\psi_m = 10$.

is based on the normalized oscillator energies $e_i = E_i/E$ which includes all terms so that $\sum_1^N E_i$ is conserved exactly

$$E_i = \tfrac{1}{2}p_i^2 + \tfrac{1}{4}[(q_{i+1} - q_i)^2 + (q_i - q_{i-1})^2] + \tfrac{1}{8}\beta[(q_{i+1} - q_i)^4 + (q_i - q_{i-1})^4]. \tag{D.4}$$

Depending on the relative variations of energies $e_{i,j}$, from one mode or oscillator to another, the values of n_{eff} or n_{osc} vary in the range from $1/N$ to 1. The upper limit corresponds to the equipartition state where all e_i and e_j are the same and equal to $1/N$. Numerical curves plotted in Fig. 15a and b, for $N = 128$ and $E = 50$ give asymptotic values at $t \to \infty$ of $n_{\text{eff}} \simeq 0.6$ and $n_{\text{osc}} \simeq 0.7$, which are lower than the upper limit values $n_{\text{osc}} = n_{\text{eff}} = 1$, as expected due to the fluctuations of energies $e_{i,j}$. In order to calculate the effect we introduce a deviation $\delta e_{i,j}$ from equipartition

$$e_{i,j} = \overline{e_{i,j}} + \delta e_{i,j}. \tag{D.5}$$

Substituting (D.5) into (D.1) or (D.3), expanding the logarithmic function, which holds both for modes and oscillators, as $\ln(1 + \delta e_i/\overline{e_i}) = \delta e_i/\overline{e_i} - \frac{1}{2}(\delta e_i/\overline{e_i})^2$ and performing the summation over i yields

$$n_{\text{eff}} = n_{\text{osc}} = \frac{1}{N}\exp\left\{-N\bar{e}\ln\bar{e} - \frac{N\overline{\delta e^2}}{2\bar{e}}\right\} = \exp\left\{-\frac{N\overline{\delta e^2}}{2\bar{e}}\right\}. \tag{D.6}$$

Taking $\bar{e} = 1/N$ and making the assumption of normal statistics that for each normal mode $\overline{\delta e^2} = \bar{e}^2$ (this is confirmed by calculations), gives an asymptotic value $n_{\text{osc}} = n_{\text{eff}} = \exp(-0.5) = 0.61$. This calculation illustrates why the result does not depend on the number of oscillators if N is sufficiently large and is in apparent good agreement with the numerical simulation for n_{eff}, but not for n_{osc}.

For an alternative perspective, we note that the sums on the RHS of (D.1) and (D.3) can be treated as ensemble averages of the function $e \ln e$ (if, of course, modes (oscillators) are statistically independent)

$$\overline{e\ln e} = \frac{1}{N}\sum_{i=1}^{i=N} e_i \ln e_i. \tag{D.7}$$

The LHS of (D.7) is calculated as a mean value of $e \ln e$ averaged over accessible states of the normal mode (oscillator) which are smoothly distributed in the phase-space due to energy exchange with the rest of the $N-1$ modes. They play the role of a heat reservoir while the total energy of the combined system is conserved. A canonical distribution can be used to describe probabilities of the different states of a single normal mode (oscillator), with a partition function Z defined by condition

$$Z = \int_{-\infty}^{\infty}\int_{-\infty}^{\infty} \exp\left\{-\frac{E_j(P,Q)}{T}\right\} \mathrm{d}P\,\mathrm{d}Q. \tag{D.8}$$

The effective temperature of the heat bath T is chosen such that $\overline{E_j} = E/N$ with E_j given by (D.2). Performing the integration over P and Q yields an expression for Z. The mean value of E_j is then calculated as

$$\overline{E_j} = \frac{1}{Z}\int_{-\infty}^{\infty}\int_{-\infty}^{\infty} E_J(P,Q) \exp\left\{-\frac{E_j(P,Q)}{T}\right\} \mathrm{d}P\,\mathrm{d}Q \equiv T. \tag{D.9}$$

Substituting these results into the integral for the mean value of $e \ln e$ yields

$$\overline{e \ln e} = \frac{1}{N}\int_0^{\infty} x \ln\left(\frac{x}{N}\right) \exp(-x)\,\mathrm{d}x. \tag{D.10}$$

Multiplying (D.10) by N and substituting in (D.1) gives an expression for the asymptotic value of n_{eff}

$$n_{\mathrm{eff}}(\infty) = \frac{1}{N}\exp[-N\overline{e \ln e}] = 0.655, \tag{D.11}$$

which slightly exceeds the numerical value 0.6 found in Fig. 15a.

In the case of oscillators, the canonical distribution has a more complicated form because the energy of each oscillator i depends on three variables $x = q_{i+1} - q_i$, $y = q_i - q_{i-1}$ and $p = p_i$. Correspondingly, expressions for Z, the mean values of E_i, and $e \ln e$ take the form

$$Z = \int_{-\infty}^{\infty}\int_{-\infty}^{\infty}\int_{-\infty}^{\infty} \exp\left\{-\frac{E_i(p,x,y)}{T}\right\} \mathrm{d}p\,\mathrm{d}x\,\mathrm{d}y, \tag{D.12}$$

$$\overline{E_i} = \frac{1}{Z}\int_{-\infty}^{\infty}\int_{-\infty}^{\infty}\int_{-\infty}^{\infty} E_i(p,x,y) \exp\left\{-\frac{E_i(p,x,y)}{T}\right\} \mathrm{d}p\,\mathrm{d}x\,\mathrm{d}y, \tag{D.13}$$

$$\overline{e \ln e} = \frac{1}{Z}\int_{-\infty}^{\infty}\int_{-\infty}^{\infty}\int_{-\infty}^{\infty} \left(\frac{E_i(p,x,y)}{E}\right) \ln\left(\frac{E_i(p,x,y)}{E}\right) \exp\left\{-\frac{E_i(p,x,y)}{T}\right\} \mathrm{d}p\,\mathrm{d}x\,\mathrm{d}y, \tag{D.14}$$

where

$$E_i(p,x,y) = \tfrac{1}{2}p_i^2 + \tfrac{1}{4}(x^2+y^2) + \tfrac{1}{8}\beta(x^4+y^4). \tag{D.15}$$

The equations are integrated numerically. Given the number of oscillators N and total energy E, the mean value of energy per oscillator $\overline{E_i}$ is found from (D.13). Equating $\overline{E_i}$ to its equipartition value, E/N, yields an appropriate effective temperature which is then used to calculate $\overline{e \ln e}$. This leads to the asymptotic value of $n_{\mathrm{osc}} = 0.74$ that again slightly exceeds the result of numerical calculations.

References

[1] A.J. Lichtenberg, M.A. Lieberman, Regular and Chaotic Dynamics, Springer, Berlin, 1992.
[2] E. Fermi, J. Pasta, S. Ulam, M. Tsingou, in: D.C. Mattis (Ed.), The Many-body Problem, World Scientific, Singapore, 1993 (reprint).

[3] J. Ford, J. Math. Phys. 2 (1961) 387.
[4] F.M. Izrailev, B.V. Chirikov, Dokl. Akad. Nauk SSSR 57 (1966) 166 [Sov. Phys. Dokl. 11 (1966) 30].
[5] P. Bocchieri, A. Scotti, B. Bearzi, A. Loinger, Phys. Rev. A 2 (1970) 2013.
[6] R. Livi, M. Pettini, S. Ruffo, M. Sparpaglione, A.Vulpiani, Phys. Rev. A 31 (1985) 1039.
[7] M. Pettini, M. Landolfi, Phys. Rev. A 41 (1990) 768.
[8] H. Kantz, R. Livi, S. Ruffo, J. Statist. Phys. 76 (1994) 627.
[9] J. DeLuca, A.J. Lichtenberg, M.A. Lieberman, Chaos 5 (1995) 283.
[10] J. DeLuca, A.J. Lichtenberg, S. Ruffo, Phys. Rev. E 51 (1995) 2877.
[11] C.F. Driscoll, T.M. O'Neil, Phys. Rev. Lett. 37 (1976) 69.
[12] C.G. Goedde, A.J. Lichtenberg, M.A. Lieberman, Physica D 57 (1992) 200.
[13] M.C. Forrest, C.G. Goedde, A. Sinha, Phys. Rev. Lett. 68 (1992) 2722.
[14] V.M. Burlakov, S.A. Kiselev, V.I. Rupasov, Phys. Lett. A 147 (1990) 130.
[15] O. Bang, M. Peyrard, Phys. Rev. E 53 (1996) 4143.
[16] J.L. Marin, S. Aubry, Nonlinearity 9 (1996) 1501.
[17] T. Cretegny, S. Aubry, S. Flach, Physica D 119 (1998) 73.
[18] T. Cretegny, T. Dauxois, S. Ruffo, A. Torcini, Physica D 121 (1998) 109.
[19] K. Ullmann, A.J. Lichtenberg, G. Corso, Phys. Rev. E 61 (2000) 2471.
[20] J. DeLuca, A.J. Lichtenberg, S. Ruffo, Phys. Rev. E 60 (1999) 3781.
[21] Yu.A. Kosevich, Phys. Rev. B 47 (1993) 3138.
[22] Yu.A. Kosevich, S. Lepri, Phys. Rev. B 61 (2000) 299.
[23] T. Dauxois, S. Ruffo, A. Torcini, Phys. Rev. E 56 (1997) R6229.
[24] A.I. D'yachenko, V.E. Zakharov, A.N. Pushkarev, V.E. Shvets, V.V. Yan'kov, Sov. Phys. JETP 69 (1989) 1144.
[25] C.F. Driscoll, T.M. O'Neil, Rocky Mt. J. Math. 8 (1978) 211.
[26] V.M. Burlakov, S.A. Kiselev, Sov. Phys. JETP 72 (1991) 854.
[27] J.L. Marin, S. Aubry, Physica D 119 (1998) 163.
[28] Yu.A. Kosevich, Phys. Rev. B 48 (1993) 3580.